Celest Mech Dyn Astr (2016) 126:89–129
DOI 10.1007/s10569-016-9702-3

ORIGINAL ARTICLE

Secular tidal changes in lunar orbit and Earth rotation

James G. Williams[1] · **Dale H. Boggs**[1]

Received: 15 January 2016 / Revised: 7 May 2016 / Accepted: 13 May 2016 /
Published online: 29 June 2016

Abstract Small tidal forces in the Earth–Moon system cause detectable changes in the orbit. Tidal energy dissipation causes secular rates in the lunar mean motion n, semimajor axis a, and eccentricity e. Terrestrial dissipation causes most of the tidal change in n and a, but lunar dissipation decreases eccentricity rate. Terrestrial tidal dissipation also slows the rotation of the Earth and increases obliquity. A tidal acceleration model is used for integration of the lunar orbit. Analysis of lunar laser ranging (LLR) data provides two or three terrestrial and two lunar dissipation parameters. Additional parameters come from geophysical knowledge of terrestrial tides. When those parameters are converted to secular rates for orbit elements, one obtains $\mathrm{d}n/\mathrm{d}t = -25.97 \pm 0.05''/\mathrm{cent}^2$, $\mathrm{d}a/\mathrm{d}t = 38.30 \pm 0.08$ mm/year, and $\mathrm{d}i/\mathrm{d}t = -0.5 \pm 0.1$ μas/year. Solving for two terrestrial time delays and an extra $\mathrm{d}e/\mathrm{d}t$ from unspecified causes gives $\sim 3 \times 10^{-12}$/year for the latter; solving for three LLR tidal time delays without the extra $\mathrm{d}e/\mathrm{d}t$ gives a larger phase lag of the N2 tide so that total $\mathrm{d}e/\mathrm{d}t = (1.50 \pm 0.10) \times 10^{-11}$/year. For total $\mathrm{d}n/\mathrm{d}t$, there is ≤ 1 % difference between geophysical models of average tidal dissipation in oceans and solid Earth and LLR results, and most of that difference comes from diurnal tides. The geophysical model predicts that tidal deceleration of Earth rotation is $-1316''/\mathrm{cent}^2$ or 87.5 s/cent^2 for UT1-AT, a 2.395 ms/cent increase in the length of day, and an obliquity rate of 9 μas/year. For evolution during past times of slow recession, the eccentricity rate can be negative.

Keywords Tides · Lunar orbit · Earth rotation · Tidal acceleration · Tidal dissipation · Moon · Lunar laser ranging (LLR)

✉ James G. Williams
James.G.Williams@jpl.nasa.gov

[1] Jet Propulsion Laboratory, California Institute of Technology, MS 238-600, Pasadena, CA 91109-8099, USA

1 Introduction

Tidal forces in the Earth–Moon system are 11 orders of magnitude weaker than the central force. The forces from tidal dissipation are another order of magnitude smaller. Nevertheless, accumulated effects of tidal dissipation cause observable changes in the lunar orbit and major evolution during the lifetime of the Earth–Moon system. Tidal dissipation in the oceans and solid Earth cause the Moon to recede from the Earth by a reported 3.81 ± 0.02 cm/year (Williams et al. 2013, 2014a). Energy and angular momentum are transferred from terrestrial spin to the lunar and solar orbits. Tides in the Moon decrease the recession rate by $\sim$1 %, but they are more important for eccentricity rate. The current secular changes in semimajor axis and eccentricity are part of long time orbit evolution. An accurate numerical integration of the lunar orbit requires a model for tidal interactions between both bodies. Lunar laser ranging (LLR) data of recent decades have accuracies from centimeters to millimeters (Samain et al. 1998; Murphy et al. 2008, 2012) and the integrated orbit that is used for analysis must be of high quality.

Satellites in low Earth orbit are strongly affected by tides in the oceans and solid Earth. At the lunar distance the tidal acceleration is feeble, allowing simpler tidal interaction models, but the model must be good enough to generate secular changes in semimajor axis, mean motion, and eccentricity along with a long period (18.6 year) modulation. The tidal model for LLR started with one Love number for tide amplitude and one angle for a geometric rotation of the tidal bulge (Williams et al. 1978). The next level of complexity used a Love number and time delay pair for each of the three frequency bands of degree-two spherical harmonics: semidiurnal (order $m = 2$), diurnal ($m = 1$), and zonal ($m = 0$) (Standish and Williams 2013). This three-band approach allowed tidal accelerations for diurnal and semidiurnal tides to be reported (Dickey et al. 1994; Williams and Boggs 2009).

This paper adds two more parameters that allow the diurnal and semidiurnal time delays to vary with frequency. The dominant tidal components within each band are not the same for semimajor axis and eccentricity change, so the frequency dependence allows the eccentricity and semimajor axis rates to be more independent and realistic. The tidal potential and the new frequency dependent model for acceleration are subjects of Sect. 2.

Degree-2 terrestrial tides can be expressed as a Fourier series containing semidiurnal, diurnal, and long periods. An expansion of the tide raising potential is given in Sect. 3. Geophysical knowledge of the Love numbers and phase shifts of an Earth with oceans is discussed in Sect. 4.

To convert the tidal Love numbers and time delays into secular rates of change for mean motion $\mathrm{d}n/\mathrm{d}t$, semimajor axis $\mathrm{d}a/\mathrm{d}t$, and eccentricity $\mathrm{d}e/\mathrm{d}t$, theoretical expressions are given and evaluated in Sect. 5. Deceleration of terrestrial spin rate is given along with obliquity rate. Three solutions for tidal acceleration parameters that fit lunar laser ranging (LLR) data are given in Sect. 6. The evaluation of these rates of change for two LLR solutions is presented in Sect. 7.

As a caution, three possible sources of unintended acceleration are described in Sect. 8. Discussions of several points follow in Sect. 9. A summary in Sect. 10 is followed by a listing of notation.

2 Tidal potential

The gravitational attraction of the Moon and Sun varies across the diameter of the Earth. In the vicinity of the Earth, the two potentials can be expressed as the sum of a potential at the

Earth's center and noncentral tidal potential terms W_2, W_3, etc. of increasing degree. Tidal forces cause the Earth to distort and that distortion generates additional potential terms V_2, V_3, etc. In this section we concentrate on the largest of the tide-raising potential terms, the degree-2 W_2, and the potential V_2 arising from the degree-2 distortion.

2.1 Theory

The degree-2 tide-raising potential from the Moon or Sun at a point at radius r from the center of the Earth is

$$W_2\,(r, \Theta) = \frac{GM' r^2}{r'^3} P_2\,(\cos\Theta) \tag{1}$$

where G is the gravitational constant, M' is the mass of tide-raising body, Θ is the Earth-centered angle between the external body and the point selected for the potential, r' is the distance from the center of the Earth to the body's center, and $r < r'$. The degree-2 unnormalized Legendre polynomial is $P_2(\cos\,\Theta) = (3\cos^2\,\Theta - 1)/2$. For tides raised by the Moon, analogous third- and higher-degree tides weaken by nearly 2 orders of magnitude ($R/r' \approx 1/60$) per degree. For the potentials in this paper, excess mass causes a positive potential and a stronger attraction, which is a common sign convention in dynamics and geodesy.

The addition theorem for unnormalized degree-2 spherical harmonic functions is

$$\begin{aligned} P_2(\cos\Theta) = {} & P_{20}(\sin\phi)\,P_{20}(\sin\phi') + \frac{1}{3} P_{21}(\sin\phi)\,P_{21}(\sin\phi')\cos(\lambda' - \lambda) \\ & + \frac{1}{12} P_{22}(\sin\phi)\,P_{22}(\sin\phi')\cos(2\lambda' - 2\lambda), \end{aligned} \tag{2}$$

where $\cos\,\Theta = \sin\,\phi\,\sin\,\phi' + \cos\,\phi\,\cos\,\phi'\,\cos(\lambda' - \lambda)$, coordinates λ and ϕ are the terrestrial longitude and latitude of a point, and primed coordinates refer to the tide raising body, which may be Moon or Sun. The latitude ϕ of a point is referred to the equator and its terrestrial longitude λ is with respect to the zero meridian. Since longitudes always appear as differences in Eq. (2), we can connect terrestrial and astronomical coordinates with $\lambda - \lambda' = \alpha - \theta - (\alpha' - \theta) = \alpha - \alpha'$, where right ascension α and Greenwich mean sidereal time θ are referred to the precessing equinox. The tide raising potential on the surface $r = R$ can be expressed as

$$\begin{aligned} W_2(R, \lambda, \phi) = {} & \frac{GM' R^2}{a'^3} \left(\frac{a'}{r'}\right)^3 \\ & \times \left[\begin{array}{l} P_{20}(\sin\phi)\,P_{20}(\sin\phi') + \frac{1}{3} P_{21}(\sin\phi)\,P_{21}(\sin\phi')\cos(\lambda' - \lambda) \\ + \frac{1}{12} P_{22}(\sin\phi)\,P_{22}(\sin\phi')\cos(2\lambda' - 2\lambda) \end{array}\right] \end{aligned} \tag{3}$$

where a' is the semimajor axis of the tide raising body. On the Earth, the 2,0 component gives rise to the long period zonal tides, the 2,1 part causes diurnal tides, and the 2,2 term causes semidiurnal tides.

For tidal distortion, first consider an Earth without oceans. For r equal to a reference radius R to the surface, the simplest form for the potential on the surface from an elastic tidal distortion of a spherically symmetric Earth is

$$V_2(R, \Theta) = k_2 W_2(R, \Theta), \tag{4}$$

where k_2 is a degree-2 Love number that depends on the elastic properties, density, and structure of the Earth. That surface potential has the shape of a degree-2 spherical harmonic

so the external potential decreases in proportion to $(R/r)^3$. Consequently, for an external point at a radius $r \geq R$, the potential from the tidal distortion is

$$V_2(r, \Theta) = \frac{k_2 G M' R^5}{r^3 r'^3} P_2(\cos\Theta). \tag{5}$$

Now Θ is the Moon or Sun centered angle between the tide-raising body and the external point at radius r. The gradient of Eq. (5) with respect to the unprimed coordinates gives acceleration. For a given radius r, tidal gravity is strongest directly toward or away from the tide-raising body where Θ is 0° or 180°.

The Earth's core-mantle boundary (CMB) is oblate and that causes the Love numbers to be frequency dependent. Equation (3) separates the tide raising potential at Earth into three frequency bands: the 2,0 zonal term gives long period tides, the 2,1 part causes diurnal tides, and the 2,2 part causes semidiurnal tides. The next approximation for V_2 uses three Love numbers k_{20}, k_{21}, and k_{22} for the three tidal bands.

$$V_2(r, \lambda, \phi) = \frac{GM' R^5}{a^3 a'^3} \left(\frac{a}{r}\right)^3 \left(\frac{a'}{r'}\right)^3 \times \left[\begin{array}{l} k_{20} P_{20}(\sin\phi) P_{20}(\sin\phi') + \frac{k_{21}}{3} P_{21}(\sin\phi) P_{21}(\sin\phi') \cos(\lambda' - \lambda) \\ + \frac{k_{22}}{12} P_{22}(\sin\phi) P_{22}(\sin\phi') \cos(2\lambda' - 2\lambda) \end{array}\right] \tag{6}$$

The Earth dissipates tidal energy. Dissipation also causes the Love number to depend on frequency and, in addition, it shifts the phase of each periodic variation in V_2 caused by W_2 variations. Models for the tidal response can be as simple as either one Love number and phase shift or time delay for each of the three bands or they can be as complicated as separate Love numbers and phase shifts for each tidal period.

The Earth's oceans do not have simple shapes. Consequently, their tidal response is more complicated than Eqs. (4–6) imply. On the surface with radius R, the tidal potential $W_2(R)$ of Eq. (3) can be expanded into a periodic series. Then the resulting external potential V_2 of Eq. (6) has a spherical harmonic expansion for each periodic term in the degree-2 series. This extensive tidal expansion is necessary when modeling the motion of artificial satellites (Petit and Luzum 2010). Owing to its distance, tidal acceleration at the Moon is small. Terms of higher degree than 2 are too weak at the Moon to be important. Terms of degree 1 affect the displacement between the center of mass of the whole Earth and the center of figure of the solid surface, but do not influence the gravity field. That leaves degree-2 terms. We are interested in secular and long period perturbations that arise from the part of the potential that has the form of Eq. (6). Consequently, we ignore most of the ocean expansion and combine degree-2 and order m solid Earth tides with ocean tides of the same degree, order, and period in what follows. As a result of the oceans and the geophysics of the Earth, the Love numbers can now depend on tidal period. Dissipation in solid Earth and oceans introduces a frequency dependent phase shift. The variation of strength and phase of the tidal response can be represented by complex Love numbers $k_2{}^*(P)$, where P is period.

2.2 Integrator model for tidal acceleration

The gradient of the potential of Eq. (6) gives the tidal acceleration that is used to numerically integrate the position of the Moon. We want a tidal model that is practical to program but complicated enough to accommodate the accuracy of the LLR data. In Standish and Williams (2013), each of the three tidal bands has a separate Love number and time delay: the Moon

or Sun coordinates r', λ', and ϕ' are evaluated at three times $t-\tau_0$, $t-\tau_1$, and $t-\tau_2$. The tidal accelerations from Moon and Sun tides are summed.

Owing to the complexity of the variation of phase lag with respect to frequency, we modify the Standish and Williams algorithm used with Eq. (6) further. We have two time delays for each of the diurnal and semidiurnal tidal bands. One we associate with daily Earth rotation and the other we associate with the slower orbital motion. The zonal tidal band has a single time delay. As explained by Folkner et al. (2014), we modify the position vector $\mathbf{r}'$ of the Moon or Sun differently for each order m

$$\mathbf{r}''_0 = \mathbf{r}'(t-\tau_0) \tag{7a}$$

$$\mathbf{r}''_m = \mathbf{R}_Z(\omega_E\tau_{Rm})\mathbf{r}'(t-\tau_m) \quad m=1,2, \tag{7b}$$

where rotation matrix $\mathbf{R}_Z$ rotates the tidal bulge on the Earth forward by angle $\omega_E\tau_m$, and ω_E is the rotation rate. There is no τ_{R0} for the zonal tides because zonal tides do not depend on longitude. Consequently, the unneeded rotation matrix for $m=0$ would be the identity matrix. We resolve $\mathbf{r}$ and $\mathbf{r}''_m$ into equatorial $\mathbf{p}$ and $\mathbf{p}''_m$ plus polar $\mathbf{z}$ and $\mathbf{z}''_m$ vectors, respectively.

$$\mathbf{r} = \mathbf{p} + \mathbf{z} \tag{8}$$

$$\mathbf{r}''_m = \mathbf{p}''_m + \mathbf{z}''_m \tag{9}$$

Then the gradient of Eq. (6) gives the acceleration of Earth and Moon; the acceleration of the Moon with respect to the Earth is

$$\frac{\mathrm{d}^2\mathbf{r}}{\mathrm{d}t^2} = \frac{3}{2}GM'\frac{(M_E+M_M)}{M_E}\left(\frac{R}{r}\right)^5 \left(\begin{array}{l} \frac{k_{20}}{r''^5_0}\left\{\begin{array}{l} 2z''^2_0\mathbf{z}+p''^2_0\mathbf{p}+r''^2_0\mathbf{r} \\ -\frac{5\left[2(zz''_0)^2+(pp''_0)^2\right]}{2r^2}\mathbf{r}\end{array}\right\} \\ +\frac{k_{21}}{r''^5_1}\left[\begin{array}{l} 2\left(\mathbf{p}\cdot\mathbf{p}''_1\right)\mathbf{z}''_1+2zz''_1\mathbf{p}''_1 \\ -\frac{10zz''_1(\mathbf{p}\cdot\mathbf{p}''_1)\mathbf{r}}{r^2}\end{array}\right] \\ +\frac{k_{22}}{r''^5_2}\left\{\begin{array}{l} 2\left(\mathbf{p}\cdot\mathbf{p}''_2\right)\mathbf{p}''_2-p''^2_2\mathbf{p} \\ -\frac{5\left[2(\mathbf{p}\cdot\mathbf{p}''_2)^2-(pp''_2)^2\right]}{2r^2}\mathbf{r}\end{array}\right\}\end{array}\right) \tag{10}$$

Mass M' refers to Moon or Sun. The trigonometric functions of λ, ϕ, and parameters modified by Eq. (7) are replaced with functions of $\mathbf{p}/r$, $\mathbf{z}/r$, $\mathbf{p}''/r''$, and $\mathbf{z}''/r''$ so that conversion between Cartesian and spherical coordinates is not necessary. Note that $z = r\sin\phi$ and z''_1 are polar components with signs, not magnitudes, so that the product zz''_1 can be positive or negative. The tidal accelerations from the lunar and solar tides are added to the other accelerations when integrating the lunar orbit (Folkner et al. 2014).

The developmental ephemeris (DE) tide model started with a single Love number and time delay (Williams et al. 1978), expanded to three pairs of Love numbers and time delays (Standish and Williams 2013), and now has three Love numbers k_{2m} and five time delays τ_{R1}, τ_{R2}, and τ_m. It is not possible to accurately solve for all of these parameters simultaneously from the LLR data. We will later discuss LLR solutions and parameters from tidal models.

3 Tidal series

The preceding subsection was concerned with an expression suitable for numerical integration. We now pursue analytical representations. Tidal variations occur at a variety of periods.

To consider frequency dependence, we expand the tidal potential W_2 at the Earth in a semi-analytical trigonometric series. In an analogous development, the tidal potential at the Moon from the Earth and Sun has been presented by Williams and Boggs (2015).

The orbit of the Moon with respect to the Earth is strongly perturbed by the Sun. The main problem of lunar theory has been the subject of considerable development. Brown's theory (Brown 1896) was the basis for his tables (Brown 1919). These were updated for the Improved Lunar Ephemeris (Eckert et al. 1954). Computer manipulation allowed the theory to be extended (Deprit et al. 1971; Henrard 1972). More recent developments (Chapront-Touzé 1983; Chapront-Touzé and Chapront 1983; Chapront and Chapront-Touzé 1996) improved accuracy leading to new tables (Chapront-Touzé and Chapront 1988, 1991). The periodic series for the lunar orbit's radius and ecliptic longitude and latitude have arguments with linear combinations of four angles

$$j_1\, l + j_2\, l' + j_3\, F + j_4\, D. \tag{11}$$

From the lunar theory, Delaunay angle l is the lunar mean anomaly (period 27.555 d), l' is the solar mean anomaly (365.260 d), F is the mean argument of latitude of the Moon (27.212 d), and D is the mean elongation of the Moon from the Sun (29.531 d). These are mean angles in the sense that polynomial expressions are used (Chapront-Touzé and Chapront 1988; Simon et al. 1994). The polynomials have small nonlinear terms due to tidal effects and the slowly changing heliocentric orbit. Truncated versions of the series for radius, and ecliptic longitude and latitude are given by Chapront-Touzé and Chapront (1988) and Chapront-Touzé and Chapront (1991). The radius is a cosine series and the longitude and latitude are sine series. The series for radius and ecliptic longitude of the Sun require the solar mean anomaly l'. The solar ecliptic latitude is zero.

The plane of the Moon's orbit is inclined by 5.145° to the ecliptic plane and the ascending node Ω is measured from the equinox along the ecliptic plane to the node. The node exhibits retrograde precession with respect to the precessing equinox with a period of 6798.38 d (18.6 year). Expressing the lunar spherical or Cartesian coordinates with respect to the equinox introduces the mean longitude $L = F + \Omega$. Although small, perturbations from the oblate Earth's gravitational J_2 also depend on the node angle Ω. The arguments of the spherical or Cartesian coordinates involve five angles.

$$\zeta_q = j_1\, l + j_2\, l' + j_3\, F + j_4\, D + j_5 \Omega, \tag{12}$$

where q is a sequential index to identify different terms in the series. The mean longitude of the Sun is $L' = L - D = F + \Omega - D$. Planetary perturbations introduce arguments with planetary longitudes, but those terms are smaller than effects considered here.

Cartesian coordinates of the Moon and Sun in the ecliptic frame are rotated by the obliquity ε to express the coordinates in the terrestrial equator frame. Six matrix functions are

$$U_{ij} = \left(\frac{a}{r}\right)^3 u_i u_j \tag{13}$$

where the u_i components of unit vector $\mathbf{r}/r$, pointing from the center of the Earth to the Moon or Sun, are calculated in a coordinate frame oriented with the first axis toward the moving equinox, the second axis 90° ahead in the equator plane, and the third axis normal to the terrestrial equator. Note that $(a/r)^3 = U_{11} + U_{22} + U_{33}$. Multiplied by $GM_M R^2/a^3$, the U_{ij} will be used to compute tidal potential. The U_{ij} matrix elements are related to tidal variations in the terrestrial moment of inertia matrix through

$$\Delta I_{ij}(t) = -\frac{k_2 M_E R^5}{a^3}\left[U_{ij} - \left(\frac{a}{r}\right)^3 \frac{\delta_{ij}}{3}\right] \tag{14}$$

where δ_{ij} is the Kronecker delta function.

The series used for the Fourier analysis are from Chapront-Touzé and Chapront (1988, 1991) plus Earth nutation terms. A five dimensional Fourier analysis of the U_{ij} was evaluated at an equally spaced grid (360°/11) of the five angles. This Fourier analysis uses five angles, not a time series, so there is no problem with close frequencies, e.g., l' (365.260 d period) separates from $2L' - l'$ (365.223 d). For later convenience, the solar U_{ij} were added on to the lunar U_{ij} with a factor of $M_S\ a^3/M_M\ a'^3 \approx 0.459$, where M_S is the solar mass, M_M is the lunar mass, a the lunar semimajor axis, and a' is the solar semimajor axis. This combination will allow one series to be used in place of two in later calculations. The largest U_{ij} coefficients are given in Table 1. Index q labels the sequence of terms in the table.

The terms with arguments $2L'$, $2L' + l'$, l', and $2L' - l'$ come mainly from the Sun. The rest of the terms, including mixtures of primed and unprimed angles, come mainly from the Moon. We say "mainly" because the distance between the Sun and Earth includes the motion of the Earth about the center of mass of the Earth–Moon system, which introduces small effects with lunar arguments. Solar perturbations of the lunar orbit cause many lunar terms with arguments containing $D = L - L'$ and l'. So arguments containing only L' and l' may be thought of as from solar Keplerian origin and those with L, l, and F, apart from F in the combination $F + \Omega - D = L'$, may be thought of as from lunar Keplerian origin. Another generality, amplitudes with arguments involving l are approximately proportional to eccentricity e and amplitudes with F, not in the combination $F + \Omega = L$, depend on inclination i. An implied sensitivity of a coefficient to a leading power of e or $\sin i$ depends on the integer factor of l or F in the argument, respectively. For example, although derived numerically, terms 3 and 4 should depend on e, terms 13 and 16 should depend on e^2, terms 5 and 6 should depend on $\sin i$ (and $\sin \varepsilon$, implied by the odd L in $L \pm F$), and term 21 should depend on $\sin^2 i$. The two strongest solar perturbation terms depend on $2D$ and $2D - l$ and these combinations are found alone (terms 8 and 12) and mixed with other angles (e.g., 7 and 9) in Table 1.

When the U_{ij} functions are rotated by angle θ into the longitude frame of the Earth, Eq. (3) for the tide raising potential at a surface point (R, λ, ϕ) becomes

$$W_2(R,\lambda,\phi) = \frac{GM_M R^2}{a'^3} \times \left\{ \begin{array}{l} P_{20}(\sin\phi)\left[U'_{33} - \frac{1}{2}\left(U'_{11} + U'_{22}\right)\right] \\ +P_{21}(\sin\phi)\left[U'_{13}\cos(\theta+\lambda) + U'_{23}\sin(\theta+\lambda)\right] \\ +\frac{1}{4}P_{22}(\sin\phi)\left[\left(U'_{11} - U'_{22}\right)\cos(2\theta+2\lambda) + 2U'_{12}\sin(2\theta+2\lambda)\right] \end{array} \right\} \quad (15)$$

Angle θ is the right ascension of the Earth's zero meridian, measured from the precessing equinox, that increases due to the daily rotation of the Earth. The primes carried over from Eq. (3) remind us that the W_2 comes from a tide raising body.

The point mass potential at the surface of the Earth is GM_E/R. Dividing by that factor and separating out the dependence on longitude λ, the Eq. (15) expression for $W_2(R, \lambda, \phi)$ can be represented as an unnormalized spherical harmonic expansion of the time varying tidal gravitational potential.

$$C_{20}^W = \frac{M_M}{M_E}\left(\frac{R}{a}\right)^3 \left[U_{33} - \frac{1}{2}\left(U_{11} + U_{22}\right)\right] \quad (16)$$

$$C_{21}^W = \frac{M_M}{M_E}\left(\frac{R}{a}\right)^3 \left[U_{23}\sin\theta + U_{13}\cos\theta\right] \quad (17)$$

Table 1 Trigonometric series are given for the combined lunar and solar U_{ij} matrix elements expressed in the equator–equinox frame

q	Argument	l	l'	F	D	Ω	$U_{11}, 10^{-6}$ cos	$U_{12}, 10^{-6}$ sin	$U_{13}, 10^{-6}$ sin	$U_{22}, 10^{-6}$ cos	$U_{23}, 10^{-6}$ cos	$U_{33}, 10^{-6}$ cos	Period days
0	0	0	0	0	0	0	730064	−1	3	615198	264947	118906	∞
1	$2L$	0	0	2	0	2	494008	453251	196486	−415857	−180274	−78151	13.661
2	$2L'$	0	0	2	−2	2	229852	210885	91430	−193484	−83884	−36368	182.621
3	$2L + l$	1	0	2	0	2	94583	86780	37620	−79620	−34516	−14963	9.133
4	l	1	0	0	0	0	81864	0	0	69019	29630	13514	27.555
5	Ω	0	0	0	0	1	0	17847	−41169	−32774	30697	32773	−6798.384
6	$L + F$	0	0	2	0	1	24	−17636	40740	32381	−30356	−32404	13.633
7	$2L + 2D - l$	−1	0	2	2	2	17965	16483	7145	−15123	−6556	−2842	9.557
8	$2D - l$	−1	0	0	2	0	15668	0	0	13212	5667	2596	31.812
9	$2L + 2D$	0	0	2	2	2	15104	13858	6008	−12715	−5512	−2389	7.096
10	$2L - l$	−1	0	2	0	2	−13965	−12813	−5554	11756	5096	2209	27.093
11	$2L' + l'$	0	1	2	−2	2	13437	12328	5345	−11311	−4904	−2126	121.749
12	$2D$	0	0	0	2	0	13354	3	1	11217	4914	2011	14.765
13	$2L + 2l$	2	0	2	0	2	12516	11483	4978	−10536	−4567	−1980	6.859
14	l'	0	1	0	0	0	11356	0	0	9559	4145	1795	365.260
15	$L + F + l$	1	0	2	0	1	2	−3378	7798	6200	−5810	−6203	9.121
16	$2l$	2	0	0	0	0	6699	0	0	5646	2429	1097	13.777
17	$2L + 2D + l$	1	0	2	2	2	3649	3348	1452	−3072	−1332	−577	5.643
18	$2L' + l$	1	0	2	−2	2	−3643	−3343	−1449	3067	1330	577	23.942
19	$\Omega + l$	1	0	0	0	1	2	1476	−3406	−2709	2540	2711	27.667
20	$\Omega - l$	−1	0	0	0	1	−2	1459	−3366	−2680	2508	2678	−27.443
21	$2F$	0	0	2	0	0	1970	−1	0	1030	2176	−3046	13.606
22	$2D + l$	1	0	0	2	0	2108	0	0	1769	779	310	9.614
23	$2\,\Omega$	0	0	0	0	2	2022	1855	806	−1702	−741	−320	−3399.19
24	$2L' - l'$	0	−1	2	−2	2	−1923	−1765	−765	1619	702	304	365.223

$$S_{21}^W = \frac{M_M}{M_E}\left(\frac{R}{a}\right)^3 [U_{23}\cos\theta - U_{13}\sin\theta] \tag{18}$$

$$C_{22}^W = \frac{1}{4}\frac{M_M}{M_E}\left(\frac{R}{a}\right)^3 [2U_{12}\sin 2\theta + (U_{11} - U_{22})\cos 2\theta] \tag{19}$$

$$S_{22}^W = \frac{1}{4}\frac{M_M}{M_E}\left(\frac{R}{a}\right)^3 [2U_{12}\cos 2\theta - (U_{11} - U_{22})\sin 2\theta] \tag{20}$$

Primes have been dropped since the tidal variations must come from the tide raising body. Since we added solar U_{ij} onto lunar U_{ij} with an appropriate scaling factor, only the lunar mass factor is needed.

Fourier analysis gives the matrix elements U_{11}, U_{22}, U_{33}, and U_{23} as cosine series $U_{ij} = \Sigma U_{ijq}\cos\zeta_q$ of angle ζ_q of Eq. (12), whereas U_{12} and U_{13} are sine series $U_{ij} = \Sigma U_{ijq}\sin\zeta_q$, where the U_{ijq} are the coefficients for each period P_q of the Fourier series for U_{ij}. Then $C_{2m}^W(t)$ and $S_{2m}^W(t)$ can also be expressed with periodic series with terms C_{2mq}^W and S_{2mq}^W. Factored by the Love number k_{2mq} for each period, the C_{2mq}^W and S_{2mq}^W terms give small unnormalized V_2 gravity field coefficients $\Delta C_{2m}(t) = \Sigma k_{2mq}\, C_{2mq}^W$ and $\Delta S_{2m}(t) = \Sigma k_{2mq}\, S_{2mq}^W$ in the terrestrial frame that can be added to the static gravity field. The individual periodic terms are

$$\Delta C_{20q} = k_{20q}\frac{M_M}{M_E}\left(\frac{R}{a}\right)^3\left[U_{33q} - \frac{1}{2}\left(U_{11q} + U_{22q}\right)\right]\cos\zeta_q \tag{21}$$

$$\begin{aligned}\Delta C_{21q} = {} & \frac{M_M}{M_E}\left(\frac{R}{a}\right)^3 \{k_{21q-}\left[U_{23q} - U_{13q}\right]\sin(\theta - \zeta_q) \\ & + k_{21q+}\left[U_{23q} + U_{13q}\right]\sin(\theta + \zeta_q)\}\end{aligned} \tag{22}$$

$$\begin{aligned}\Delta S_{21q} = {} & \frac{M_M}{M_E}\left(\frac{R}{a}\right)^3 \{k_{21q-}\left[U_{23q} - U_{13q}\right]\cos(\theta - \zeta_q) \\ & + k_{21q+}\left[U_{23q} + U_{13q}\right]\cos(\theta + \zeta_q)\}\end{aligned} \tag{23}$$

$$\Delta C_{22q} = \frac{1}{8}\frac{M_M}{M_E}\left(\frac{R}{a}\right)^3 \left\{\begin{array}{l} k_{22q-}\left[U_{11q} - U_{22q} + 2U_{12q}\right]\cos(2\theta - \zeta_q) \\ +k_{22q+}\left[U_{11q} - U_{22q} - 2U_{12q}\right]\cos(2\theta + \zeta_q)\end{array}\right\} \tag{24}$$

$$\Delta S_{22q} = \frac{1}{8}\frac{M_M}{M_E}\left(\frac{R}{a}\right)^3 \left\{\begin{array}{l} k_{22q-}\left[U_{11q} - U_{22q} + 2U_{12q}\right]\sin(2\theta - \zeta_q) \\ +k_{22q+}\left[U_{11q} - U_{22q} - 2U_{12q}\right]\sin(2\theta + \zeta_q)\end{array}\right\} \tag{25}$$

Except for the constant term with $q = 0$, each frequency in the U_{ij} series generates two frequencies for each of the diurnal and semidiurnal tides. Including the zonal tides, there are five tidal arguments $m\theta \pm \zeta_q$ with five frequencies for each U_{ij} argument ζ_q (three each for q=0). A $\pm$ in the $k_{2mq\pm}$ subscript associates subscript $2mq-$ with argument $m\theta' - \zeta_q'$ and $2mq+$ with $m\theta' + \zeta_q'$. With dissipation, replace $k_{2mq\pm}$ with complex $k_{2mq\pm}{}^*$ to derive the tidal field V_2 generated by the distorted Earth. Then $\mathrm{Re}(k_{2mq\pm}{}^*) = |k_{2mq\pm}{}^*|\cos(\chi_{2mq\pm})$ and $\mathrm{Im}(k_{2mq\pm}{}^*) = -|k_{2mq\pm}{}^*|\sin(\chi_{2mq\pm})$, where the $\chi_{2mq\pm}$ are phase shifts (lags) for each term. Replace $k_{2mq\pm}$ in the above expressions (Eqs. 20–25) by R times complex displacement Love number $h_{2mq\pm}{}^*$ to get the spherical harmonic coefficients for the vertical tidal distortion of the Earth's surface. Phase lags $\chi_{2mq\pm}$ have the same signs as the rates for arguments $m\theta \pm \zeta_q$. Most arguments have positive rates and positive $\chi_{2mq\pm}$, but a few negative rates (and $\chi_{2mq\pm}$) for zonal tides ($m = 0$) involve the retrograde precessing node Ω.

Values of parameters used in tidal calculations are given in Table 2. The lunar semimajor axis comes from the inverse time averaged value $1/a = \langle 1/r\rangle$, which is different from the

Table 2 Values of parameters used in tidal calculations

Parameter	Value
R	6378.136 km
M_E/M_M	81.300569
M_S/M_E	332946.0488
GM_M	4902.80007 km^3/s^2
Lunar a	384399.0 km
Lunar e	0.0549
Lunar i	5.145°
Lunar n	17325593.4″/year
Solar a'	149598023 km
Solar n'	1295977.4″/year
C/MR^2	0.33070
k_{2f}	0.93
h_{2f}	1.93

average of osculating values. The first five values in the table come from the DE430 ephemeris (Williams et al. 2013; Folkner et al. 2014). The equatorial radius is used instead of the mean radius. The sidereal mean motions in seconds of arc per Julian year are n for the Moon and n' for the Sun; polynomial expressions for lunar and solar angles are found in Chapront-Touzé and Chapront (1988), Simon et al. (1994), and Chapront et al. (2002). With $R/a \approx 1/60.268$ and $M_M/M_E \approx 1/81.3006$, the coefficient $(M_M/M_E)(R/a)^3$ is 5.619×10^{-8}. When that coefficient is multiplied by equatorial radius R, the factor of 0.3584 m has the dimensions of length. These two factors scale the size of terrestrial tidal effects for gravity field coefficients and displacements, respectively. For the Earth without oceans, the real Love numbers are $k_2 \approx 0.300$ and $h_2 \approx 0.608$. In Petit and Luzum (2010), see Tables 6.5 for $k_{2m}*$ and 7.2 for $h_{2m}*$ at the different tidal frequencies. Fluid Love numbers are k_{2f} and h_{2f}.

The zonal or long period tides involve the declination and radial motions of the Moon or Sun. The zonal 2,0 tides slowly modulate a tidal contribution to the oblateness of the Earth. Table 3 gives series for the zonal spherical harmonic coefficients of the tide raising potential W_2 and the product RW_2 that is needed for radial tides. The precession rates of Earth satellites are modulated by tidal changes of $\Delta C_{20}(t)$. The polar moment of inertia, I_{33} of Eq. (14), is also modulated by $\Delta C_{20}(t)$ causing tidally driven variations in Earth rotation (Yoder et al. 1981; Ray and Erofeeva 2014).

The constant tide contributes a small addition to the oblate shape caused by spin. Using a fluid Love number of $k_{2f} = 0.93$, tides cause 2.9×10^{-8} of the $J_2 = 1.0826 \times 10^{-3}$, or 0.0027 %. For shape, the figures are 57 cm in equator to pole flattening using h_{2f} =1.93. With the elastic Love number h_2 increasing from 0.61 at 2 weeks period to 0.63 at 18.6 years (Petit and Luzum 2010), there are five zonal tides with amplitudes between 1 and 3 cm. The 2-week Mf tide and the 6-month Ssa tide are caused by latitude variations, whereas the monthly Mm tide is caused by orbit eccentricity.

In the arguments of Tables 1 and 3 we use positive angles θ, L, and Ω, which are referred to the precessing equinox. This causes terms 5 and 20 to have negative rates. The tidal community commonly uses positive rates reversing the sign of these two arguments. Our Doodson numbers reflect this difference, 55,545 versus 55,565 and 45,645 versus 65,465. Since Tables 1 and 3 use cosine series, this sign difference should not cause a problem for W_2, but it should be kept in mind when applying a phase shift for V_2.

Table 3 Zonal or long period tidal components of W_2 and RW_2 with amplitudes of RC^W_{20q} >1 mm

q	Argument	l	l'	F	D	Ω	Ampl. RC^W_{20q} mm	Ampl. C^W_{20q} 10^{-10}	Period days	Doodson Number	Tide ID
0	0	0	0	0	0	0	−198.44	−311.13	∞	55,555	const
1	$2L$	0	0	2	0	2	−42.01	−65.87	13.6608	75,555	Mf
2	$2L'$	0	0	2	−2	2	−19.55	−30.65	182.6209	57,555	Ssa
3	$2L + l$	1	0	2	0	2	−8.04	−12.61	9.1329	85,455	Mtm
4	l	1	0	0	0	0	−22.19	−34.80	27.5546	65,455	Mm
5	Ω	0	0	0	0	1	17.62	27.62	−6798.3840	55,545	
6	$L + F$	0	0	2	0	1	−17.42	−27.31	13.6334	75,565	
7	$2L + 2D - l$	−1	0	2	2	2	−1.53	−2.40	9.5569	83,655	
8	$2D - l$	−1	0	0	2	0	−4.24	−6.65	31.8119	63,655	
9	$2L + 2D$	0	0	2	2	2	−1.28	−2.01	7.0958	93,555	Msqm
10	$2L - l$	−1	0	2	0	2	1.19	1.86	27.0925	65,655	
11	$2L' + l'$	0	1	2	−2	2	−1.14	−1.79	121.7493	58,554	
12	$2D$	0	0	0	2	0	−3.68	−5.77	14.7653	73,555	
13	$2L + 2l$	2	0	2	0	2	−1.06	−1.67	6.8594	95,355	
14	l'	0	1	0	0	0	−3.10	−4.87	365.2596	56,554	Sa
15	$L + F + l$	1	0	2	0	1	−3.33	−5.23	9.1207	85,465	
16	$2l$	2	0	0	0	0	−1.82	−2.85	13.7773	75,355	
19	$\Omega + l$	1	0	0	0	1	1.46	2.28	27.6667	65,445	
20	$\Omega - l$	−1	0	0	0	1	1.44	2.26	−27.4433	45,645	
21	$2F$	0	0	2	0	0	−1.63	−2.55	13.6061	75,575	

The product h_{20q} * RC^W_{20q} gives the tide height component and k_{20q} * C^W_{20q} gives the potential coefficient component from distortion. The cosine series of the 2,0 spherical harmonic is multiplied by the latitude function $P_{20}(\sin\phi) = (3\sin^2\phi - 1)/2$

The diurnal tides involve the declination motion as well as the longitude and radius motions of the Moon or Sun. They have maximum size at $\phi = \pm 45°$ and are zero at the poles and on the equator. A periodic term with argument $\theta - L$ (1.03505 d period) would be aligned with the mean lunar direction whereas argument $\theta - L'$ (1 day) would be aligned with the mean solar direction. Neither argument occurs among the diurnal tides given in Table 4 although term 14 with argument $\theta - l'$ is very close to the solar day period, but does not have the same phase. A period that is slower than 1.03505 days acts like a wave moving westward with respect to the mean lunar longitude and a period slower than 1 day moves westward with respect to the mean solar longitude. Equations (22) and (23) have two periodic terms for each ζ_q. The largest diurnal waves have arguments $\theta - \zeta_q$, but smaller terms with arguments $\theta + \zeta_q$ are also tabulated in Table 4. Note that the maximum variation of a 2,1 periodicity is $P_{21}(\pm 1/\sqrt{2}) = \pm 1.5$ times the coefficients from Eqs. (22) and (23).

Important diurnal tides include the K1 tide at 1 sidereal day (0.9973 d), the lunar O1 and solar P1 tides, and the Q1 tide. The tide with argument $\theta - \Omega$ is a sideband of the K1 tide and the tide with argument $\theta - L - F$ is a sideband of the O1 tide. The angle between the equator and lunar orbit planes varies between $\varepsilon + i$ and $\varepsilon - i$, which gives rise to the sidebands.

The semidiurnal tides have maximum variation on the equator and are null at the poles. The maximum variation of a semidiurnal periodicity is $P_{22}(0) = 3$ times the tabulated coefficients from Eqs. (24) and (25). The large M2 tide with argument $2\theta - 2L$ (period 0.517525 d) has two lobes aligned with the mean lunar longitude and the 0.5 day S2 tide with argument $2\theta - 2L'$ follows the Sun. Waves with longer periods move westward with respect to those two directions and shorter periods move eastward. The K2 tide occurs at half of the sidereal rotation period and the N2 tide is also important. The semidiurnal waves with arguments $2\theta - \zeta_q$ dominate in Table 5; only one small term with argument $2\theta + \zeta_q$ is tabulated. A longer list of tidal amplitudes is available from Hartmann and Wenzel (1995).

4 Model Love numbers for the Earth with oceans

In order to use the tidal acceleration from Eq. (10), we need to assess the influence of the oceans as well as the underlying body of the Earth on the combined Love numbers $k_2{}^*(P)$ and their associated time delays. The real part of $k_2{}^*$ is largely from the body of the Earth, but the dissipation caused imaginary part is mainly from the oceans (Ray et al. 2001).

A geophysical assessment of Love numbers is given in Table 6. The model Love numbers for Earth (without oceans) comes from tables in Petit and Luzum (2010) and the ocean model is from FES2004 (Lyard et al. 2006), tabulated as Stokes parameters (ftp://tai.bipm.org/iers/convupdt/chapter6/tidemodels/fes2004_Cnm-Snm.dat). The real and imaginary components of $k_2{}^*$ are given separately for the body of the Earth, the oceans, and their sum. The phase shift for each component comes from the arctangent of the imaginary part divided by the real part. The smaller real Love number and positive imaginary part for the body K1 tide is due to a nearby resonance from the oblate CMB. The K1 tide is a major tide that affects Earth rotation, but it is not important for tidal acceleration of mean longitude. The real part has a very small influence on mean motion and precession rates.

The real and imaginary parts of the combined $k_2{}^*$ from Table 6 are shown as circular spots in Fig. 1. A constant time delay would cause the imaginary spots to lie along a straight line descending from the origin, and the long period spots do trend downward, but the figure shows more structure with the imaginary values in the diurnal and semidiurnal bands trending

Table 4 Diurnal tidal components of W_2 and RW_2 with amplitudes of $RC^W_{21q\pm}$ >2/3 mm

q	Argument	θ	l	l'	F	D	Ω	Ampl. RC^W_{21q} mm	Ampl. C^W_{21q} 10^{-10}	Period days	Doodson Number	Tide ID
0	θ	1	0	0	0	0	0	94.95	148.87	0.9973	165,555	K1
1	$\theta - 2L$	1	0	0	−2	0	−2	−67.51	−105.85	1.0758	145,555	O1
	$\theta + 2L$	1	0	0	2	0	2	2.90	4.55	0.9294	185,555	Oo1
2	$\theta - 2L'$	1	0	0	−2	2	−2	−31.41	−49.25	1.0027	163,555	P1
	$\theta + 2L'$	1	0	0	2	−2	2	1.35	2.12	0.9919	167,555	ϕ 1
3	$\theta - 2L - l$	1	−1	0	−2	0	−2	−12.93	−20.27	1.1195	135,655	Q1
4	$\theta - l$	1	−1	0	0	0	0	5.31	8.32	1.0347	155,655	M1
	$\theta + l$	1	1	0	0	0	0	5.31	8.32	0.9624	175,455	J1
5	$\theta - \Omega$	1	0	0	0	0	−1	12.88	20.19	0.9971	165,565	
	$\theta + \Omega$	1	0	0	0	0	1	−1.88	−2.94	0.9974	165,545	
6	$\theta - L - F$	1	0	0	−2	0	−1	−12.74	−19.97	1.0760	145,545	
	$\theta + L + F$	1	0	0	2	0	1	1.86	2.92	0.9293	185,565	
7	$\theta - 2L - 2D + l$	1	1	0	−2	−2	−2	−2.46	−3.85	1.1135	137,455	
8	$\theta - 2D + l$	1	1	0	0	−2	0	1.02	1.59	1.0295	157,455	
	$\theta + 2D - l$	1	−1	0	0	2	0	1.02	1.59	0.9670	173,655	
9	$\theta - 2L - 2D$	1	0	0	−2	−2	−2	−2.06	−3.24	1.1603	127,555	
10	$\theta - 2L + l$	1	1	0	−2	0	−2	1.91	2.99	1.0354	155,455	
11	$\theta - 2L' - l'$	1	0	−1	−2	2	−2	−1.84	−2.88	1.0055	162,556	π 1
12	$\theta - 2D$	1	0	0	0	−2	0	0.88	1.38	1.0695	147,555	
	$\theta + 2D$	1	0	0	0	2	0	0.88	1.38	0.9342	183,555	
13	$\theta - 2L - 2l$	1	−2	0	−2	0	−2	−1.71	−2.68	1.1669	125,755	2Q1
14	$\theta - l'$	1	0	−1	0	0	0	0.74	1.16	1.0000	164,556	S1
	$\theta + l'$	1	0	1	0	0	0	0.74	1.16	0.9946	166,554	Ψ1

Table 4 continued

q	Argument	θ	l	l'	F	D	Ω	Ampl. RC^W_{21q} mm	Ampl. C^W_{21q} 10^{-10}	Period days	Doodson Number	Tide ID
15	$\theta - L - F - l$	1	−1	0	−2	0	−1	−2.44	−3.82	1.1197	135,645	
19	$\theta - \Omega - l$	1	−1	0	0	0	−1	1.07	1.67	1.0346	155,665	
20	$\theta - \Omega + l$	1	1	0	0	0	−1	1.05	1.65	0.9623	175,465	

The multiplying latitude spherical harmonic is $P_{21}(\sin\phi) = 3 \sin\phi \cos\phi$ and the longitude functions are cos λ with a sine series and sin λ with a cosine series; see Eqs. (22) and (23)

Table 5 Semidiurnal tidal components of W_2 and RW_2 with amplitudes of $RC^W_{22q\pm}$ >1/3 mm

q	Argument	θ	l	l'	F	D	Ω	Ampl. RC^W_{22q} mm	Ampl. C^W_{22q} 10^{-10}	Period days	Doodson Number	Tide ID
0	2θ	2	0	0	0	0	0	10.29	16.14	0.4986	275,555	K2
1	$2\theta - 2L$	2	0	0	−2	0	−2	81.37	127.57	0.5175	255,555	M2
2	$2\theta - 2L'$	2	0	0	−2	2	−2	37.86	59.36	0.5000	273,555	S2
3	$2\theta - 2L - l$	2	−1	0	−2	0	−2	15.58	24.42	0.5274	245,655	N2
4	$2\theta - l$	2	−1	0	0	0	0	0.58	0.90	0.5078	265,655	
	$2\theta + l$	2	1	0	0	0	0	0.58	0.90	0.4898	285,455	
5	$2\theta - \Omega$	2	0	0	0	0	−1	3.07	4.81	0.4986	275,565	
6	$2\theta - L - F$	2	0	0	−2	0	−1	−3.03	−4.75	0.5176	255,545	
7	$2\theta - 2L - 2D + l$	2	1	0	−2	−2	−2	2.96	4.64	0.5261	247,455	
9	$2\theta - 2L - 2D$	2	0	0	−2	−2	−2	2.49	3.90	0.5363	257,555	
10	$2\theta - 2L + l$	2	1	0	−2	0	−2	−2.30	−3.61	0.5080	265,455	L2
11	$2\theta - 2L' - l'$	2	0	−1	−2	2	−2	2.21	3.47	0.5007	272,556	
13	$2\theta - 2L - 2l$	2	−2	0	−2	0	−2	2.06	3.23	0.5377	235,755	2N2
15	$2\theta - L - F - l$	2	−1	0	−2	0	−1	−0.58	−0.91	0.5275	245,645	
17	$2\theta - 2L - 2D - l$	2	−1	0	−2	−2	−2	0.60	0.94	0.5470	227,655	
18	$2\theta - 2L' - l$	2	−1	0	−2	2	−2	−0.60	−0.94	0.5092	263,655	
23	$2\theta - 2\Omega$	2	0	0	0	0	−2	0.33	0.52	0.4986	275,575	

The multiplying latitude spherical harmonic is $P_{22}(\sin\phi)$=3 $\cos^2\phi$ and the longitude functions are $\cos(2\lambda)$ with a cosine series and $-\sin(2\lambda)$ with a sine series; see Eqs. (24) and (25)

Table 6 The real and imaginary parts of potential Love numbers from body, ocean, and combined tides are listed for 13 major tidal components

Tide	Body Re k_2*	Body Im k_2*	Ocean Re k_2*	Ocean Im k_2*	Total Re k_2*	Total Im k_2*	Total $\lvert k_2 * \rvert$	Lag χ	Time delay day
Ssa	0.3059	−0.0032	0.0263	−0.0010	0.3323	−0.0041	0.3323	0.71°	0.360
Mm	0.3027	−0.0024	0.0375	−0.0066	0.3402	−0.0090	0.3403	1.51°	0.116
Mf	0.3017	−0.0021	0.0333	−0.0098	0.3350	−0.0119	0.3351	2.03°	0.077
Mtm	0.3012	−0.0020	0.0300	−0.0107	0.3312	−0.0127	0.3314	2.19°	0.056
Q1	0.2978	−0.0014	0.0239	−0.0226	0.3217	−0.0240	0.3226	4.26°	0.0132
O1	0.2975	−0.0014	0.0205	−0.0220	0.3180	−0.0234	0.3189	4.20°	0.0126
P1	0.2869	−0.0007	0.0176	−0.0161	0.3045	−0.0168	0.3050	3.16°	0.0088
K1	0.2575	+0.0012	0.0175	−0.0162	0.2750	−0.0150	0.2754	3.12°	0.0086
2N2	0.3011	−0.0013	−0.0108	−0.0328	0.2903	−0.0341	0.2923	6.69°	0.0100
N2	0.3011	−0.0013	−0.0186	−0.0308	0.2825	−0.0321	0.2843	6.49°	0.0095
M2	0.3011	−0.0013	−0.0199	−0.0237	0.2811	−0.0250	0.2822	5.07°	0.0073
S2	0.3010	−0.0013	−0.0171	−0.0171	0.2840	−0.0184	0.2846	3.71°	0.0052
K2	0.3010	−0.0013	−0.0164	−0.0175	0.2846	−0.0188	0.2852	3.77°	0.0052

Magnitudes, phase lags χ, and equivalent time delays follow. The tidal components are ordered by decreasing period

upward with frequency. The downward deflection of the real k_2* in the diurnal band illustrates the CMB resonance.

To represent the tides that are important for the Moon's orbit during an integration and solution, we have a choice of three Love numbers and five time delays. We cannot solve for all of these parameters so we take some values from the Table 6 geophysical model and solve for others. During LLR solutions, we fix the three Love numbers and either two delays τ_0 and τ_1 or three delays τ_0, τ_1, and τ_2. Then the tidal acceleration in longitude allows us to solve for the remaining time delays τ_2, τ_{R1}, and τ_{R2}, or else for τ_{R1} and τ_{R2}, respectively. The diurnal τ_{R1} and semidiurnal τ_{R2} delays can be separately estimated because they cause 18.6 year modulations of dn/dt as well as secular rates. This modulation occurs because the inclination of the lunar orbit to the equator varies between $\varepsilon - i$ and $\varepsilon + i$ during the 18.6 year precession of the node along the ecliptic plane (Williams et al. 1978). Solutions with three time delays are also sensitive to eccentricity rate. The most important tides for orbit evolution are the fortnightly Mf, the diurnal O1 and Q1, and the semidiurnal M2 and N2 tides (Sect. 5.3). Consequently, we attempt to match those five tides, subject to modification by the LLR solution. In decreasing order of importance are the M2, O1, and N2 tides for acceleration in longitude and the N2, Q1, M2, and 2N2 tides for eccentricity rate.

For an initial estimate of time delays, we use the geophysical model of Table 6 for the M2, N2, O1, Q1, and Mf tides as follows:

(a) For the zonal tides, we match the Mf tide with magnitude $k_{20} = 0.335$ and time delay $\tau_0 = 0.077$ d. These values do not match the other smaller components closely. The eccentricity rate from the Mm tide will be underestimated, but it is small compared to the diurnal and semidiurnal values. The single time delay causes the imaginary part of k_{20} to be zero at zero tidal frequency.

(b) For diurnal tides, the O1 tide is strongest for dn/dt and the Q1 tide is strongest for de/dt. Consequently, we pick $k_{21} = 0.320$. Then time delays $\tau_1 = -0.008$ d and $\tau_{R1} = 0.0110$ d result from solving two equations of the form $k_{21} \sin(\omega_E \tau_{R1}\text{-}\mathrm{d}\zeta_q/\mathrm{d}t\ \tau_1) = -\mathrm{Im}(k_{21q}{}^*)$ with the imaginary Love numbers for the O1 and Q1 entries in Table 6. The small τ_1 value results from the small difference in imaginary Love numbers.

(c) The M2 tide is strongest for semidiurnal dn/dt and the N2 tide is strongest for de/dt. With $k_{22} = 0.283$, two equations of the form $k_{22} \sin(2\omega_E \tau_{R2}\text{-}\mathrm{d}\zeta_q/\mathrm{d}t\ \tau_2) = -\mathrm{Im}(k_{22q}{}^*)$ yield $\tau_2 = -0.112$ d and $\tau_{R2} = 0.00294$ d. The negative values of τ_1 and τ_2 reflect the increase in their $-\mathrm{Im}(k_{2mq}{}^*)$ components with period rather than a response to the future position of the Moon as Eq. (7) implies.

The above three choices for the real and imaginary k_2* are shown as solid lines in Fig. 1.

We have adopted the model Love numbers for solid Earth from Table 6.5 in Petit and Luzum (2010) and the ocean model from FES2004 (Lyard et al. 2006). The long period zonal tides are difficult to measure. The treatment by Ray and Erofeeva (2014) has larger imaginary components than we have used. Since the zonal tides contribute <1 % of the tidal acceleration (Sect. 5.3) this difference is not critical, but improvement is possible.

5 Secular rates for spin, obliquity, and orbit

The gravity from the lunar and solar tidal deformations acts back on the Moon and Sun. There results a transfer of energy and angular momentum to the lunar and solar orbits from

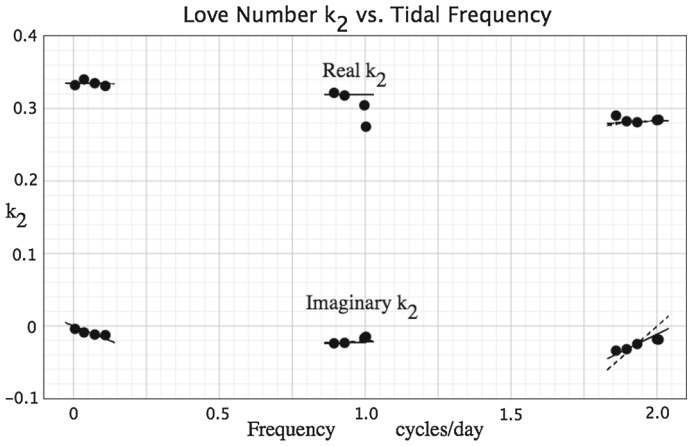

Fig. 1 The real and imaginary terrestrial k_2* for 13 major tides from Table 6 are shown as *filled circles*. The values in the long period, diurnal, and semidiurnal bands are approximated with functions shown as *solid lines* for the geophysical model and *dashed lines* for solution D of Table 9

the Earth's spin. A secular decrease in terrestrial spin rate and an increase in lunar distance is a consequence of phase lags caused by tidal dissipation.

Equation (6) for the potential V_2 from the tidal distortion (before introducing dissipation) depends on products of spherical harmonic functions. An equivalent expression depends on products of the U_{ij} functions. We seek the potential of Moon and Sun raised tides acting back on the Moon and Sun. With the U_{ij} expressed as trigonometric series with amplitudes U_{ijq}, the products will have a large number of periodic terms with sums and differences of the frequencies in the U_{ij} series. Since we are interested in secular rates, we select products of terms with the same periods that give constant argument differences ($\theta - \theta'$ and $\zeta_q - \zeta'_q$) and zero frequencies.

$$\mathrm{V}_{20} = \frac{GM_M R^5}{8a^3 a'^3} \sum_q \left(1+\delta_{q0}\right) k_{20q} \left[U_{11q} + U_{22q} - 2U_{33q}\right] \times \left[U'_{11q} + U'_{22q} - 2U'_{33q}\right] \cos\left(\zeta_q - \zeta'_q\right) \tag{26a}$$

$$\mathrm{V}_{21} = \frac{3GM_M R^5}{4a^3 a'^3} \sum_q \left(1+\delta_{q0}\right) \times \left[\begin{array}{l} k_{21q-}\left(U_{13q} - U_{23q}\right)\left(U'_{13q} - U'_{23q}\right)\cos\left(\theta - \zeta_q - \theta' + \zeta'_q\right) \\ +k_{21q+}\left(U_{13q} + U_{23q}\right)\left(U'_{13q} + U'_{23q}\right)\cos\left(\theta + \zeta_q - \theta' - \zeta'_q\right) \end{array}\right] \tag{26b}$$

$$V_{22} = \frac{3GM_M R^5}{16a^3 a'^3} \sum_q \left(1+\delta_{q0}\right) \times \left[\begin{array}{l} k_{22q-}\left(U_{11q} - U_{22q} + 2U_{12q}\right)\left(U'_{11q} - U'_{22q} + 2U'_{12q}\right)\cos\left(2\theta - \zeta_q - 2\theta' + \zeta'_q\right) \\ +k_{22q+}\left(U_{11q} - U_{22q} - 2U_{12q}\right)\left(U'_{11q} - U'_{22q} - 2U'_{12q}\right)\cos\left(2\theta + \zeta_q - 2\theta' - \zeta'_q\right) \end{array}\right] \tag{26c}$$

The Kronecker delta function δ_{q0} compensates for fewer multiplications of sines and cosines due to fewer independent arguments when $\zeta_0 = \zeta'_0 = 0$. Also, when $q = 0$ for the diurnal and

semidiurnal potentials (K1 and K2 tides), two terms combine. The primes refer to the tides distorting the Earth whereas unprimed parameters result from the action on the Moon and Sun. Partial derivatives below only apply to unprimed parameters. Dissipation will originate from the primed tide raising part and we now include a prime on θ' in combinations $m\theta' \pm \zeta'_q$. Numerically, the linear combinations of U_{ijq} amplitudes enter as squares. The same combinations enter in Eqs. (21–25).

We allow the Love number and phase to depend on tidal frequency. A $\pm$ has been added to their subscripts to associate subscripts $2mq-$ with argument $m\theta' - \zeta'_q$ and $2mq+$ with $m\theta' + \zeta'_q$. With a phase lag $\chi_{2mq\pm}$, then

$$k_{2mq\pm} \sin \chi_{2mq\pm} = k_{2mq\pm} \sin \left(m\theta \pm \zeta_{2mq\pm} - m\theta' \mp \zeta'_{2mq\pm} \right) = -\mathrm{Im}\left(k_{2mq\pm}*\right) \quad (27)$$

5.1 Earth rotation and orientation rates

The torque acting to decelerate the Earth's rotation about its polar axis is given by the partial derivative of potential energy $M_M V_2$ with respect to θ, $T_E = M_M \partial V_2/\partial\theta$. In V_2 of Eq. (26), we differentiate with respect to the θ in $m\theta \pm \zeta$, but not the θ' in the $m\theta' \pm \zeta'$ from the tide raising potential. Multiplying one series times another gives many periodic terms, but for secular deceleration, a sine and cosine pair of terms with the same period multiply one another. The main secular effects result from the lunar tides acting back on the Moon and the solar tides acting back on the Sun. Except for the constant, K1, and K2 tides from both Sun and Moon, the products of mixed solar and lunar terms mainly give periodic torques. We assume that the core and mantle decelerate together. The tidal acceleration of the Earth's rotation is $\mathrm{d}^2\theta/\mathrm{d}t^2 \approx \mathrm{d}\omega_E/\mathrm{d}t = T_E/S_W C(\omega_E)$, where T_E is torque, the polar principal moment of inertia is $C(\omega_E)$, and spin rate is ω_E. Angle θ is referred to the precessing equinox, which direction along the ecliptic plane has a small (right-handed) tide induced acceleration of order 0.2 milliarcseconds/cent^2 (mas/cent^2) (Williams 1994) and a larger classical acceleration of about $-2.2''/\mathrm{cent}^2$ (Hilton et al. 2006).

$$\frac{\mathrm{d}\omega_E}{\mathrm{d}t} = -\frac{3}{8}\frac{GM_M^2}{M_E a^3}\left(\frac{R}{a}\right)^3 \frac{M_E R^2}{S_W C(\omega_E)} \sum_q \left(1+\delta_{q0}\right) \times \left\{ \begin{array}{l} 2\left[U_{13q} - U_{23q}\right]^2 k_{21q-} \sin\chi_{21q-} \\ +2\left[U_{13q} + U_{23q}\right]^2 k_{21q+} \sin\chi_{21q+} \\ +\left[U_{11q} - U_{22q} + 2U_{12q}\right]^2 k_{22q-} \sin\chi_{22q-} \\ +\left[U_{11q} - U_{22q} - 2U_{12q}\right]^2 k_{22q+} \sin\chi_{22q+} \end{array} \right\} \quad (28)$$

We have combined the lunar and solar U_{ij} functions and Eq. (26) is written for that case. If the solar and lunar U_{ij} had been kept separate, then we would have needed a second term that replaced M_M and a with their solar counterparts. The squares of all periodic tidal components give deceleration of spin.

At long time scales, the Earth's shape is close to hydrostatic equilibrium with a moment of inertia tensor that depends on a spherical component plus an oblate component that is proportional to ω_E^2. A slower spinning Earth is both less oblate, depending on the degree-2 fluid Love number in Table 2, and its radius shrinks, depending on a degree-0 coefficient (Yoder et al. 1981). With $\mathrm{d}[C(\omega_E)\omega_E]/\mathrm{d}t = S_W C(\omega_E)\mathrm{d}\omega_E/\mathrm{d}t$, the factor $S_W = 1.005$ allows for the small dependence of the moment of inertia on spin rate.

The factors for spin change from each imaginary Love number are tabulated in Table 7. Multiply the tabulated values by $k_{2mq\pm} \sin \chi_{2mq\pm} = -\mathrm{Im}(k_{2mq\pm}{}^*)$ for each periodic term. The M2 tide dominates the deceleration of Earth rotation, but the S2, K1, and O1 tides are also major contributors. The zonal tides do not affect rotation about the polar axis.

Most of the Earth's current $-0.468''$/year decrease of obliquity is due to motion of the ecliptic plane rather than motion of the equator plane. Still, space referenced obliquity change can evolve through higher time derivatives. However, a small space referenced obliquity rate of -0.268 mas/year is caused by lunar torques on the Earth's static figure; the lunar orbit plane precesses along a plane that is slightly offset from the ecliptic plane (Williams 1994). The tidal torque on the Earth is $-M_M \mathbf{r} \times \nabla V_2$. One can compute the contribution of tidal torques to secular obliquity rate by dividing the torque component about the Earth's Y axis (in the equator plane 90° ahead of the equinox direction) by the Earth's angular momentum $C\omega_E$, $\mathrm{d}\varepsilon/\mathrm{d}t = (M_M/C\omega_E)\,(u_1 \partial V_2/\partial u_3 - u_3 \partial V_2/\partial u_1)$, where the potential comes from Eq. (26). This angular momentum approximation is not quite the same as solving the Euler equations for the body's $\mathrm{d}\varepsilon/\mathrm{d}t$, but it is close for small perturbations. Selecting the secular terms, the contribution from each spherical harmonic component summed over each periodic tidal term is

$$\frac{\mathrm{d}\varepsilon_{20}}{\mathrm{d}t} = -\frac{3}{4}\frac{GM_M^2}{M_E a^3}\left(\frac{R}{a}\right)^3 \frac{M_E R^2}{C\omega_E} \sum_q \left(1+\delta_{q0}\right) U_{13q} \left[U_{11q} + U_{22q} - 2U_{33q}\right] k_{20q} \sin \chi_{20q} \tag{29a}$$

$$\frac{\mathrm{d}\varepsilon_{21}}{\mathrm{d}t} = \frac{3}{4}\frac{GM_M^2}{M_E a^3}\left(\frac{R}{a}\right)^3 \frac{M_E R^2}{C\omega_E} \sum_q \left(1+\delta_{q0}\right) \times \begin{bmatrix} \left(U_{11q} - U_{33q} + U_{12q}\right)\left(U_{13q} - U_{23q}\right) k_{21q-} \sin \chi_{21q-} \\ -\left(U_{11q} - U_{33q} - U_{12q}\right)\left(U_{13q} + U_{23q}\right) k_{21q+} \sin \chi_{21q+} \end{bmatrix} \tag{29b}$$

$$\frac{\mathrm{d}\varepsilon_{22}}{\mathrm{d}t} = \frac{3}{8}\frac{GM_M^2}{M_E a^3}\left(\frac{R}{a}\right)^3 \frac{M_E R^2}{C\omega_E} \sum_q \left(1+\delta_{q0}\right) \times \begin{bmatrix} \left(U_{13q} - U_{23q}\right)\left(U_{11q} - U_{22q} + 2U_{12q}\right) k_{22q-} \sin \chi_{22q-} \\ -\left(U_{13q} + U_{23q}\right)\left(U_{11q} - U_{22q} - 2U_{12q}\right) k_{22q+} \sin \chi_{22q+} \end{bmatrix} \tag{29c}$$

Unlike most periodic tides, the K1 and K2 tidal terms do not split up with multiple phases, hence the Kronecker delta function δ_{q0}. The zonal term from $q = 0$ can be ignored. The above secular expressions are valid with our combined lunar and solar U_{ij}. For separate lunar and solar U_{ij}, originally in each expression the first U_{ij} combination was unprimed and the second was primed, one $1/a^3$ was primed, and one mass factor was primed. For secular terms from solar U_{ij}, the M_M^2 is replaced with M_S^2 and $1/a^6$ is replaced with solar $1/a'^6$.

The contributions from each tidal component are tabulated in Table 7. The table shows that the K1, O1, and M2 tides give the largest obliquity rates. The M2 and O1 tides give positive rates while the K1 tide causes a negative rate. Consequently, the total rate can depend on the details of dissipation vs. period. The constant, K1, and K2 tides ($q = 0$) may be thought of as arising from a ring of mass in the ecliptic plane. Shifting the phase of a corresponding tidal ring causes small torques about the $-$Y and $-$Z axes.

In Table 7 arguments containing $L + F$ are related to $2L$ terms (Mf, O1, and M2) modified by the precessing inclined lunar orbit plane and arguments with Ω are similarly related to the constant, K1, and K2 terms. Although many terms are nearly Keplerian, terms with arguments containing $2D$ and $2D - l$ come from solar perturbations of the lunar orbit.

Table 7 Secular tidal effects on Earth rotation, obliquity rate, and lunar orbital elements from zonal, diurnal, and semidiurnal tides

Tide	Argument	$d\omega_E/dt$ ″/cent^2	$d\varepsilon/dt$ μas/year	dn/dt ″/cent^2	da/dt mm/year	de/dt 1×10^{-12}/year	di/dt μas/year
Mf	$2L$	0	−45.1	9.4	−13.9	0.5	0.2
Ssa	$2L'$	0	−9.8	0	0	0	0
Mm	l	0	0	1.3	−1.9	−45.4	0
Mtm	$2L + l$	0	−1.7	0.5	−0.8	−5.9	0
	$L + F$	0	−3.9	1.6	−2.4	0.1	−3.5
	Ω	0	−4.0	0	0	0	3.6
Other	Zonal	0	−0.1	0.2	−0.2	−1.0	−0.4
K1	θ	−6312	−634.2	0	0	0	0
O1	$\theta - 2L$	−3191	378.3	−145.8	215.1	−7.6	−2.6
P1	$\theta - 2L'$	−691	81.9	0	0	0	0
Q1	$\theta - 2L - l$	−117	13.9	−8.0	11.8	92.1	−0.1
	$\theta - L - F$	−114	1.0	−5.2	7.7	−0.3	11.3
	$\theta - \Omega$	−116	1.0	0	0	0	−11.6
M1	$\theta - l$	−20	−2.0	−0.4	0.7	15.6	0
J1	$\theta + l$	−20	−2.0	0.4	−0.7	−15.6	0
	$\theta - 2L - 2D + l$	−4	0.5	−0.3	0.4	−3.4	0.8
	$\theta - 2L - 2D$	−3	0.4	−0.3	0.4	0	0.6
Other	Diurnal	−23	−2.5	−0.2	0.2	6.5	0.4
K2	2θ	−593	−59.6	0	0	0	0
M2	$2\theta - 2L$	−37086	335.0	−847.3	1249.7	−44.2	−15.0
S2	$2\theta - 2L'$	−8028	72.5	0	0	0	0

Table 7 continued

Tide	Argument	$d\omega_E/dt$ ″/cent^2	$d\varepsilon/dt$ μas/year	dn/dt ″/cent^2	da/dt mm/year	de/dt 1×10^{-12}/year	di/dt μas/year
N2	$2\theta - 2L - l$	−1359	12.3	−46.6	68.2	535.0	−0.6
	$2\theta - L - F$	−51	−2.4	−1.2	1.7	−0.1	2.6
	$2\theta - \Omega$	−53	−2.4	0	0	0	−2.6
	$2\theta - 2L - 2D + l$	−49	0.4	−1.7	2.5	−19.5	4.9
	$2\theta - 2L - 2D$	−35	0.3	−1.6	2.3	−0.1	3.4
L2	$2\theta - 2L + l$	−30	0.3	−0.3	0.5	−11.7	0
	$2\theta - 2L' - l'$	−27	0.2	0	0	0	0
2N2	$2\theta - 2L - 2l$	−24	0.2	−1.1	1.6	18.8	0
Other	Semidiurnal	−10	−0.5	−0.2	0.3	2.3	0.1

Multiply rates by $k_{2mq} \sin \chi_{2mq}$ = -Im(k_{2mq}*)

5.2 Lunar orbit rates

Lagrange's form of the perturbation equations gives secular rates for n, a, e, and i as functions of $\partial V_2/\partial l$, $\partial V_2/\partial \omega$, and $\partial V_2/\partial \Omega$, where ω is argument of perigee. With two finite masses, the relative acceleration has a factor of $1 + M_M/M_E$. For first order perturbations, we take the partials with respect to the mean angles l, ω, and Ω in the tidal arguments using $L = \Omega + \omega + l$, $F = \omega + l$, and $D = L - L'$. For the tide caused lunar secular semimajor axis rate

$$\frac{\mathrm{d}a}{\mathrm{d}t} = \frac{naS_A}{2}\frac{M_M}{M_E}\left(\frac{R}{a}\right)^5 \sum_q j_{Mq} \left\{ \begin{array}{l} -\frac{1}{2}\left[U_{11q} + U_{22q} - 2U_{33q}\right]^2 k_{20q} \sin\chi_{20q} \\ +3\left[U_{23q} - U_{13q}\right]^2 k_{21q-} \sin\chi_{21q-} \\ -3\left[U_{23q} + U_{13q}\right]^2 k_{21q+} \sin\chi_{21q+} \\ +\frac{3}{4}\left[U_{11q} - U_{22q} + 2U_{12q}\right]^2 k_{22q-} \sin\chi_{22q-} \\ -\frac{3}{4}\left[U_{11q} - U_{22q} - 2U_{12q}\right]^2 k_{22q+} \sin\chi_{22q+} \end{array} \right\} \quad (30)$$

Integer j_{Mq} is the sum of integers multiplying monthly angles l, F, and D in the angle ζ_q. For example, the Mf, O1, Oo1 and M2 terms have $j_{Mq} = 2$ and the Q1 and N2 terms have $j_{Mq} = 3$. The K1, K2 and pure solar terms like Ssa, P1, and S2 are excluded by $j_{Mq} = 0$.

In lunar theory it is possible to modify Kepler's third law to include most of the effect of the mean attraction of the Sun.

$$G\,(M_E + M_M) = n^2 a^3 \left(1 + \frac{n'^2}{2n^2}\right) \quad (31)$$

The values of the semimajor axis and sidereal mean motion are given in Table 2; neither one is the mean value of the osculating element. At first order, the tabulated value of a is larger than its mean osculating value by a factor of $1 + n'^2/2n^2$ whereas sidereal n is smaller than its mean osculating value by the factor $1 - n'^2/n^2$. The ratio of solar to lunar sidereal mean motions is n'/n = 1/13.3687 so $n'^2/2n^2$ = 0.0028. Perturbations of secular semimajor axis and mean motion rates are connected through the derivative of Eq. (31).

$$\frac{\mathrm{d}n}{\mathrm{d}a} = -\frac{3n}{2a}\left(1 + \frac{n'^2}{2n^2}\right) \quad (32)$$

The perturbed secular rates for dn/dt and da/dt in Table 7 should be multiplied by the $k_{2mq} \sin\chi_{2mq}$ value for each period. When constructing the table, the U_{ij} are evaluated with the R and a parameters in Table 2, but the n and a parameters that appear in the differential equations need to be adjusted. The differential Eq. (30) for da/dt is corrected by the factor S_A = 1 + 2n'^2/n^2 = 1.0112. Then the dn/dt differential equation would have a factor of the product S_N = 1 + 5$n'^2/2n^2$ = 1.0140. The second order perturbations (tidal vs. solar perturbations) are probably the largest source of error in the conversion of the imaginary Love numbers into the secular rates for dn/dt and da/dt. The error would be some uncertain fraction of n'^2/n^2 = 0.0056. We can get some idea of the conversion accuracy by comparing the three results for a simple model. Williams et al. (1978) presented an early tidal acceleration model for a geometrical bulge rotated by a small angle $\Delta\theta$. With the foregoing S_N factor, the 1978 expression for dn/dt in "/cent^2 is $-1954\ k_2\Delta\theta$. The same acceleration model in Chapront-Touzé and Chapront (1988) gave $-1957\ k_2\Delta\theta$, and the numerical expressions of this paper give $-1961\ k_2\ \Delta\theta''$/cent^2. Although there are differences in the three derivations, we adopt a conversion error of 0.15 % for dn/dt and da/dt, which is about $n'^2/4n^2$.

The secular perturbations for tidal eccentricity and inclination rates are also given in Table 7. In Eq. (30) replace $a\ S_A\ j_{Mq}$ with $S_E\ [j_{Mq}\ (1 - e^2) - j_{Wq}\ \sqrt{(1 - e^2)}]/2e$ to get de/dt, where the integer factor j_{Wq} of ω is the sum of integer multipliers of F and D in ζ_q.

To get di/dt replace with $S_E\ [j_{Wq}\cos i - j_{\Omega q}]/[2\sin i\sqrt{(1-e^2)}]$, where j_Ω is the integer factor for Ω in a tidal argument.

$$\frac{\mathrm{d}e}{\mathrm{d}t} = \frac{nS_E}{4e}\frac{M_M}{M_E}\left(\frac{R}{a}\right)^5 \sum_q \Big[j_{Mq}\left(1-e^2\right) - j_{Wq}\sqrt{1-e^2}\Big] \begin{Bmatrix} -\frac{1}{2}\left[U_{11q}+U_{22q}-2U_{33q}\right]^2 k_{20q}\sin\chi_{20q} \\ +3\left[U_{23q}-U_{13q}\right]^2 k_{21q-}\sin\chi_{21q-} \\ -3\left[U_{23q}+U_{13q}\right]^2 k_{21q+}\sin\chi_{21q+} \\ +\frac{3}{4}\left[U_{11q}-U_{22q}+2U_{12q}\right]^2 k_{22q-}\sin\chi_{22q-} \\ -\frac{3}{4}\left[U_{11q}-U_{22q}-2U_{12q}\right]^2 k_{22q+}\sin\chi_{22q+} \end{Bmatrix} \tag{33}$$

$$\frac{\mathrm{d}i}{\mathrm{d}t} = \frac{nS_E}{4\sin i\sqrt{1-e^2}}\frac{M_M}{M_E}\left(\frac{R}{a}\right)^5 \sum_q \left[j_{Wq}\cos i - j_{\Omega q}\right] \begin{Bmatrix} -\frac{1}{2}\left[U_{11q}+U_{22q}-2U_{33q}\right]^2 k_{20q}\sin\chi_{20q} \\ +3\left[U_{23q}-U_{13q}\right]^2 k_{21q-}\sin\chi_{21q-} \\ -3\left[U_{23q}+U_{13q}\right]^2 k_{21q+}\sin\chi_{21q+} \\ +\frac{3}{4}\left[U_{11q}-U_{22q}+2U_{12q}\right]^2 k_{22q-}\sin\chi_{22q-} \\ -\frac{3}{4}\left[U_{11q}-U_{22q}-2U_{12q}\right]^2 k_{22q+}\sin\chi_{22q+} \end{Bmatrix} \tag{34}$$

Both differential equations are factored by $S_E = 1 + n'^2/2n^2 = 1.0028$. For the eccentricity e and inclination i we use the values in Table 2. The osculating eccentricity varies by tens of percent due to solar perturbations and an appropriate characteristic value is unclear and may vary with the term. Consequently, we suggest that the conversion for eccentricity rate may be uncertain by several percent. We divide the constant part of the product of U functions by a constant eccentricity, but a more accurate procedure would have divided the full secular plus periodic series from the product of U functions by the osculating eccentricity before extracting the secular rates.

Some terms occur as opposing pairs: Table 7 shows that M1 and J1 (arguments $\theta \pm l$) are opposites for all perturbations except spin and obliquity rate, whereas terms with arguments $L + F$ and $L - F = \Omega$ have opposing effects in inclinations. Other pairings of coefficients can be recognized in Table 1, e.g., terms 17 and 18 ($2L + l \pm 2D$), and also 19 and 20 ($\Omega \pm l$). Such pairs arise when the product of two trigonometric functions give functions with sums and differences of the two arguments.

In addition to low order perturbations of n, a, e, and i, there are second order perturbations that cause accelerations of longitude of perigee ϖ and node Ω. The solar perturbations dominate the precession rates of these two elements and these rates depend on n, e, and i. The tidal rates for n, e, and i will cause accelerations of ϖ and node Ω. The partial derivatives are given by Chapront-Touzé and Chapront (1983) and Chapront-Touzé and Chapront (1988). The dominant partials of these accelerations are with respect to dn/dt, -0.014818 for acceleration of $\bar{\omega}$ and 0.003746 for Ω. Although our paper reports tidal acceleration of (sidereal) mean longitude dn/dt, the tidal acceleration of mean anomaly is dl/d$t \approx 1.0148$ dn/dt and the acceleration of argument of latitude is dF/d$t \approx 0.9963$ dn/dt.

Tides only weakly affect the annual orbit of the Earth–Moon system about the Sun. In Eq. (30), lunar parameters can be replaced with solar parameters. Then secular changes of semimajor axis and mean longitude are

$$\frac{\mathrm{d}a'}{\mathrm{d}t} = 0.019(k_2\sin\chi)_{P1} + 0.112(k_2\sin\chi)_{S2}\ \text{mm/year} \tag{35}$$

$$a' \frac{\mathrm{d}n'}{\mathrm{d}t} = -0.182(k_2 \sin\chi)_{P1} - 1.055(k_2 \sin\chi)_{S2} \text{ mm/year}^2 \quad (36)$$

With the lagged components $(k_2 \sin\chi)_{P1} = -\mathrm{Im}(k_2{}^*)_{P1} = 0.0170$ and $(k_2 \sin\chi)_{S2} = -\mathrm{Im}(k_2{}^*)_{S2} = 0.0184$ from Table 6, one gets $\mathrm{d}a'/\mathrm{d}t = 2.4$ μm/year and $a'\mathrm{d}n'/\mathrm{d}t = -23$ μm/year^2. After ±1 decade, the affect on the solar longitude component is −1 mm.

5.3 Tidal rates from model Love numbers

Applying the model Love numbers of Table 6 to the perturbation factors of Table 7 yields the results for $\mathrm{d}\omega_E/\mathrm{d}t$, $\mathrm{d}\varepsilon/\mathrm{d}t$, $\mathrm{d}n/\mathrm{d}t$, $\mathrm{d}e/\mathrm{d}t$, and $\mathrm{d}i/\mathrm{d}t$ in Table 8. The sum of the diurnal components for deceleration of spin gives $-189''$/cent^2, the semidiurnal sum is $-1136''$/cent^2, and the total is $-1325''$/cent^2. The tidal contribution to the obliquity rate is very small at 9 μas/year. For $\mathrm{d}n/\mathrm{d}t$ the zonal tides cause $+0.15''$/cent^2, diurnal tides cause $-3.74''$/cent^2, and semidiurnal tides produce $-22.83''$/cent^2. The terrestrial total is $-26.42''$/cent^2. The N2 tide dominates the eccentricity rate followed by the Q1 and M2 contributions. The inclination change is very small. In addition to the table, tides on the Moon contribute a small positive acceleration to $\mathrm{d}n/\mathrm{d}t$ and negative eccentricity rate. For terrestrial tides, the ratio of deceleration of rotation to orbital deceleration is 50.1. Christodoulidis et al. (1988) predicted a ratio of 49. Although the ratios of 50.6 for diurnal and 49.7 for semidiurnal decelerations are similar, the zonal ratio is zero and there is no single ratio that is consistent across all components. Earth rotation in seconds of arc can be converted to seconds of UT1 by dividing by $-15.043''$/s.

We note that a decreasing polar moment of inertia also causes the spin rate to change (Yoder et al. 1983), which causes the measured deceleration to be less than the tidal deceleration (Stephenson and Morrison 1995). Polar moment changes are proportional to J_2 changes (Yoder et al. 1983; Cheng et al. 2013).

The total tidal obliquity rate from Table 8 is 9.2 μas/year. The M2 and O1 tides give positive rates for $\mathrm{d}\varepsilon/\mathrm{d}t$ while the K1 rate is negative. The rates from the diurnal tides nearly cancel at 1.0 μas/year, whereas the semidiurnal tides contribute a positive rate of 8.9 μas/year. Zonal tides cause −0.7 μas/year. Previously, an obliquity rate of 24 μas/year was computed by Williams (1994) who assumed that a conserved component of spin angular momentum was normal to the ecliptic plane. This approximation assumed that the tidal forces are in the ecliptic plane. However, phase shifts for the rotating Earth cause small out-of-plane forces that violate the assumption. A positive obliquity rate from the M2 tide was derived by Kaula (1964). An obliquity rate of 11.5 μas/year was derived by Mignard (1981) for a 10 min time delay. A 9.63 μas/year rate was computed by Krasinsky (1999). Rubincam (2016) noted that the semidiurnal tide with a positive obliquity rate acts opposite a negative diurnal rate. His obliquity rate would be a few μas/year positive.

The IAU theory for precession and obliquity (Hilton et al. 2006) uses observed values for the precession and obliquity motion of the equator with respect to space to set the J2000 values. Although the Williams (1994) tidal obliquity rate was used for part of the time dependence in the IAU theory, with the total rate specified it (or any other tidal rate) only slightly affects the derivation of the higher degree polynomial coefficients. The total theoretical obliquity rate is −268 μas/year from orbit orientation (Williams 1994) plus 9.2 μas/year from tides yielding −259 μas/year. A rate of −252.4 μas/year was determined by VLBI (Mathews et al. 2002) and corrected to −257.5 μas/year by Capitaine et al. (2003), allowing for the displacement of the equinox from the origin of the IAU right ascension and declination. The latter rate was used by Hilton et al. for the IAU2006 precession theory. There is good agreement between the theoretical and observed values. For time scales >10,000 year, the −268 μas/year is variable taking either sign whereas the 9 μas/year is secular, albeit subject to variation due

Table 8 Secular rates for $\mathrm{d}\omega_E/\mathrm{d}t$, $\mathrm{d}\varepsilon/\mathrm{d}t$, $\mathrm{d}n/\mathrm{d}t$, $\mathrm{d}e/\mathrm{d}t$, and $\mathrm{d}i/\mathrm{d}t$ using the imaginary part of the model Love numbers from Table 6

Tide	Argument	$\mathrm{d}\,\omega_E/\mathrm{d}t$ ″/cent^2	$\mathrm{d}\,\varepsilon/\mathrm{d}t$ μas/year	$\mathrm{d}n/\mathrm{d}t$ ″/cent^2	$\mathrm{d}e/\mathrm{d}t$ 10^{-12}/year	$\mathrm{d}i/\mathrm{d}t$ μas/year
Mf	$2L$	0	−0.5	0.11	0.01	0
Ssa	$2L'$	0	0	0	0	0
Mm	l	0	0	0.01	−0.41	0
Mtm	$2L+l$	0	0	0.01	−0.08	0
	$L+F$	0	0	0.02	0	−0.04
Other	Zonal	0	0	0	−0.01	0.02
K1	θ	−94.5	−9.5	0	0	0
O1	$\theta-2L$	−74.4	8.8	−3.41	−0.18	−0.1
P1	$\theta-2L'$	−11.6	1.4	0	0	0
Q1	$\theta-2L-l$	−2.8	0.3	−0.19	2.21	0
M1	$\theta-l$	−0.4	0	−0.01	0.32	0
J1	$\theta+l$	−0.4	0	0.01	−0.28	0
	$\theta-L-F$	−2.7	0	−0.12	−0.01	0.3
	$\theta-\Omega$	−1.7	0	0	0	−0.2
Other	Diurnal	−0.5	0	−0.02	0.04	0
K2	2θ	−11.1	−1.1	0	0	0
M2	$2\theta-2L$	−925.7	8.4	−21.15	−1.10	−0.4
S2	$2\theta-2L'$	−148.0	1.3	0	0	0
N2	$2\theta-2L-l$	−43.7	0.4	−1.50	17.19	0
	$2\theta-L-F$	−1.3	−0.1	−0.03	0	0.1
	$2\theta-\Omega$	−1.0	0	0	0	−0.1
	$2\theta-2L-2D+l$	−1.6	0	−0.05	−0.62	0.2
	$2\theta-2L-2D$	−1.2	0	−0.05	0	0.1
L2	$2\theta-2L+l$	−0.6	0	−0.01	−0.26	0
	$2\theta-2L'-l'$	−0.5	0	0	0	0
2N2	$2\theta-2L-2l$	−0.8	0	−0.04	0.64	0
Other	Semidiurnal	−0.2	0	−0.01	0.07	0

The orbital perturbations from tides on the Moon are not included

to the changing phases of the O1, K1, and M2 tides. For evolutionary times, only the latter accumulates.

The decreasing terrestrial spin has a tidal power drain of $C\omega_E\ \mathrm{d}\omega_E/\mathrm{d}t$. There is also tidal energy dissipation from the zonal tides; that energy must come from the lunar orbit rather than spin. Hence, there is a positive $\mathrm{d}n/\mathrm{d}t$ (negative $\mathrm{d}a/\mathrm{d}t$) for zonal tides in Table 8. The power going into the lunar orbit is $(GM_EM_M/2a^2)\ \mathrm{d}a/\mathrm{d}t$ and the power deposited in the solar orbit is $[G(M_E+M_M)M_S/2a'^2]\ \mathrm{d}a'/\mathrm{d}t$. The power difference between spin and orbit is dissipated. With the model values from Table 8, terrestrial tides extract an average 3.78×10^{12} watts from the Earth's rotation while depositing 1.22×10^{11} watts in the lunar orbit and $\sim1.4\times10^{10}$ watts in the solar orbit so that 3.64×10^{12} watts is dissipated. Examination of the imaginary parts of the Love numbers in Table 6 shows that ∼95 % of the energy dissipation is in the oceans and ∼5 % is in the solid Earth.

6 LLR solutions

The Lunar Laser Ranging (LLR) experiment measures the time of flight of a laser pulse fired from an observatory on the Earth toward a retroreflector on the Moon and bounced back to the observatory. It is convenient to multiply these time-of-flight observations by the speed of light and call them ranges. Data are processed from McDonald Observatory, Texas; Observatoire de la Côte d'Azur, France (Samain et al. 1998); Haleakala Observatory, Hawaii; Apache Point Observatory, New Mexico (Murphy et al. 2008, 2012); and Matera, Italy. LLR data are available from the International Laser Ranging Service archive at http://ilrs.gsfc.nasa.gov/. There are five target retroreflector arrays on the Moon. These flat arrays of corner cubes are located at the Apollo 11, 14, and 15 landing sites and on the Lunokhod 1 and 2 rovers. The Apollo 15 array at the Hadley site is the largest; it provides the strongest returned signal and the majority of ranges. See reviews by Dickey et al. (1994) and Murphy (2013) for further descriptions.

In addition to the terrestrial and lunar tidal time delays of this paper, the weighted least squares fits of LLR data include solution parameters for ranging station coordinates, reflector coordinates, initial conditions for the integration of the lunar orbit and rotation, $G(M_E+M_M)$, Earth orientation including precession rate, obliquity rate, and nutation, lunar tidal potential time delay τ_M and displacement Love number h_{2M}, dissipation at its core-mantle boundary (CMB), and other parameters. The lunar orbit in lunar and planetary ephemeris DE430 (Williams et al. 2013; Folkner et al. 2014) resulted from analysis of 18,548 lunar ranges from March 1970 to December 2012. Table 9 tabulates the Love number and time delay values used for DE430 and two new solutions of this paper. Tabulated quantities with uncertainties are fit. Lunar Love number k_{2M} comes from GRAIL determinations (Konopliv et al. 2013; Lemoine et al. 2013; Williams et al. 2014b). Dissipation at the lunar CMB depends on LLR solution parameter K_V/C_M, where the torque between the fluid and mantle is proportional to K_V and the polar moment is C_M (Williams et al. 2001). Lunar τ_M and K_V/C_M are mainly determined by effects on the physical librations (Williams et al. 2001) and they are highly correlated (−0.998) in solutions because they both contribute to a large term in the pole direction. A linear combination, $1.2 \times 10^{-7}\tau_M + K_V/C_M \approx 2.9 \times 10^{-8}$, is determined better than the separate parameters. The τ_M and K_V/C_M determinations separate fairly well from the terrestrial time delays during solutions; the diurnal and semidiurnal correlations are moderate for solution D.

New solutions analyze 20,218 lunar ranges from March 1970 to September 2015. Since DE430 was created there have been improvements to the lunar and terrestrial models including tidal displacements, tidally driven UT1 and polar motion variations, atmospheric delay, and lunar tidal effects on lunar physical librations (Williams and Boggs 2015). As a consequence of model improvements and new data, the rms residuals/uncertainties of the weighted least squares fits are reduced by ∼5 % since DE430 was created. For solutions A and B, three fixed terrestrial Love numbers and time delays are taken from Sect. 4. Solution A did not solve for an extra de/dt whereas solution B did. Solution C solves for τ_2 instead of an extra de/dt. Solution D iterated the fits and integrations and then fixed τ_2 at −0.200 d. Tide and dissipation related parameters are presented for solutions B and D in Table 9. In Fig. 1, the dependence of Love number on tidal frequency is shown for solution B with solid lines while the dependence for solution D is indicated with dashed lines.

The uncertainties produced by the least squares procedure depend on the choice of solution parameters. Solution B with an extra de/dt gives a significant value and a 0.6 % better fit than solution A without it. Solution C that solves for τ_2 instead of solution B's extra de/dt is an

Table 9 Tide related Love numbers and time delays used for DE430 and new LLR solutions

Parameter	DE430	New solution B	New solution D
k_{20}	0.335	0.335	0.335
τ_0	0.064 d	0.077 d	0.077 d
k_{21}	0.320	0.320	0.320
τ_{R1}	0.00736 ± 0.00030 d	0.01021 ± 0.00028 d	0.01024 ± 0.00028 d
τ_1	−0.044 d	−0.008 d	−0.008 d
k_{22}	0.320	0.283	0.283
τ_{R2}	0.002535 ± 0.000025 d	0.002882 ± 0.000028 d	-0.00037 ± 0.00124 d
τ_2	−0.100 d	−0.113 d	-0.200 ± 0.033 d
Lunar k_{2M}	0.024059	0.024059	0.02422
Lunar τ_M	0.0958 ± 0.0109 d	0.115 ± 0.021 d	0.120 ± 0.021 d
Lunar K_V/C_M	$(1.637 \pm 0.135) \times 10^{-8}$/d	$(1.58 \pm 0.26) \times 10^{-8}$/d	$(1.44 \pm 0.25) \times 10^{8}$ /d
Extra de/dt	0	$(3.43 \pm 1.27) \times 10^{-12}$/year	0

equally acceptable fit that allows the N2 perturbation to absorb the extra rate, but the resulting N2 phase shift of 7.6° deviates from the geophysically based 6.5° in Table 6. The DE430 solution, without an extra de/dt, results in a smaller lunar delay τ_M, a larger K_V/C_M, and smaller uncertainties for both. Like DE430, solution A (not shown) also has a smaller τ_M and a larger K_V/C_M. The correlation between τ_{R1} and τ_{R2} is −0.908 for DE430 and −0.672 for solution B; over all solutions increasing one delay is partly compensated by decreasing the other so that the total dn/dt changes little. The uncertainties in Table 9 include the effects of correlations. The uncertainties shown for solution D come from solution C to better represent realistic uncertainties. Changing τ_2 also caused τ_M and K_V/C_M to change. When selecting τ_2 we considered the consistency of τ_M with other lunar tidal dissipation parameters that are sensitive to monthly dissipation (Williams and Boggs 2015); solution D with solution C's uncertainty has $k_{2M}/Q = (6.7 \pm 1.1) \times 10^{-4}$. Some DE430 lunar parameter uncertainties are smaller than those of the new solutions because of a smaller set of solution parameters.

Our partial derivative for extra eccentricity rate follows from approximate semianalytical expressions.

$$r \approx a\left[1 + \frac{1}{2}e^2 - e\cos l - 0.175e\cos(2D - l) - 0.077\cos(2D)\right] \tag{37}$$

$$\Delta r = a\left[e - \cos l - 0.175\cos(2D - l)\right]\frac{\mathrm{d}e}{\mathrm{d}t}\Delta t \tag{38}$$

The perturbed radius is Δr and Δt is the time elapsed since a reference time. Our partial derivative uses the two periodic terms in Eq. (38), but not the constant ae de/dt Δt term. During discussions with D. Pavlov (private communication 2015) we discovered that our former analytical partial was deficient by a factor of two. Consequently, our previously reported values and uncertainties for extra de/dt (Williams and Boggs 2009; Williams et al. 2014a) should be divided by two. Since the physical cause of the extra de/dt was unspecified, it was not present in our past numerically integrated ephemerides. Adjusting τ_2 would allow future ephemerides to include the extra eccentricity rate.

The LLR solutions also give the obliquity motion with respect to space. Solution D finds an Earth rotation rate about the direction of zero right ascension and declination of 284 ±

34 μas/year. With the small correction for the displacement of the equinox in Capitaine et al. (2003), this gives an obliquity motion with respect to space of -288 ± 34 μas/year, agreeing within its uncertainty with the theoretical value (Sect. 5.3) and the VLBI value adopted for the IAU2006 precession (Hilton et al. 2006). The rates from DE430 and solution B are similar.

7 Tidal rates from LLR solutions

When the tidal parameters of Table 9 are used with the acceleration model of the numerical integrations, then the tidal influences are implicit in the resulting ephemeris. However, we would like to know the tide induced changes in lunar mean motion n, semimajor axis a, eccentricity e, and inclination i. For that, we use the numerical theory from Sect. 5. The theory for element rates from tides on the Moon is presented in Sect. 8 of Williams et al. (2001). The resulting tidal changes are given in Table 10. Overall, tides on the Moon and zonal tides on Earth tend to shrink the orbit and its eccentricity whereas diurnal and semidiurnal tides tend to expand the orbit and eccentricity. The M2 tide accounts for 81 % of the change in semimajor axis whereas the N2 tide dominates the eccentricity change. In decreasing order of importance are the M2, O1, and N2 tides for $\mathrm{d}n/\mathrm{d}t$ and $\mathrm{d}a/\mathrm{d}t$ whereas for eccentricity rate the N2, anomalistic lunar tide, Q1, and M2 tides are important. Inclination change is very small.

At the end of Table 10 there are two sets of uncertainties. The first set is intended to describe a realistic (not formal) internal uncertainty based on the LLR least squares fits. For DE430 the internal uncertainties should apply to the numerically integrated ephemeris, which also has a systematic 2×10^{-12}/year eccentricity rate error. However, we see that adjusting τ_2 has altered the rates by more than the expected uncertainties. Consequently, a dynamical model giving $\mathrm{d}e/\mathrm{d}t$ is not identical to an analytical $\mathrm{d}e/\mathrm{d}t$. Most of the uncertainties for eccentricity and inclination rates come from tides on the Moon. The second line of uncertainties includes the estimated error of converting the tidal solution parameters to mean element rates as discussed in Sect. 5.2.

A summary of secular rates is presented in Table 11 for the geophysical model of Table 6, ephemeris DE430, and new LLR solutions B and D of Table 9. Solution B has $\mathrm{d}n/\mathrm{d}t$ and $\mathrm{d}a/\mathrm{d}t$ close to the DE430 values, but the magnitudes of $\mathrm{d}a/\mathrm{d}t$ and $\mathrm{d}n/\mathrm{d}t$ are slightly larger for solution D and $\mathrm{d}e/\mathrm{d}t$ is larger due to the effect of the altered τ_2 on the N2 contribution. Note that the smaller DE430 lunar τ_M absorbed about 1/3 of the extra rate found for solution B in Table 9.

When the terrestrial $\mathrm{d}n/\mathrm{d}t$ and $\mathrm{d}a/\mathrm{d}t$ rates in Tables 10 and 11 are compared with rates from the geophysical model (Tables 8, 11), we find that the geophysical model has 1.0 % larger magnitudes for DE430 and solution B and is 0.7 % larger than solution D. These differences are compatible with an earlier comparison by Williams and Boggs (2009). Most of the difference comes from the diurnal contribution, that geophysical value is 7 to 9 % larger than the LLR values. Since we have put the LLR and geophysical results through the same conversion, the differences should not be significantly affected by conversion error.

Previously reported DE430 secular rates (Williams et al. 2013, 2014a) were computed from an analytical theory based on a precessing elliptical orbit. Periodic solar perturbation terms were ignored. Those previous rates were different by $0.08''/\mathrm{cent}^2$ for $\mathrm{d}n/\mathrm{d}t$ and -0.12 mm/year for $\mathrm{d}a/\mathrm{d}t$, partly due to the missing solar perturbation terms with arguments $2\theta - 2L - 2D + l$ and $2\theta - 2L - 2D$.

Table 10 Tidal rates of change for lunar mean motion n, semimajor axis a, eccentricity e, and inclination i using parameters from Table 9

Tide	DE430 dn/dt $''/cent^2$	DE430 da/dt mm/year	DE430 de/dt 10^{-12}/year	DE430 di/dt μas/year	Soln D dn/dt $''/cent^2$	Soln D da/dt mm/year	Soln D de/dt 10^{-12}/year	Soln D di/dt μas/year
Zonal								
Mf	0.09	−0.14	0.01	0	0.11	−0.16	0.01	0
Mm	0.01	−0.01	−0.22	0	0.01	−0.01	−0.27	0
Mtm	0.01	−0.01	−0.09	0	0.01	−0.01	−0.10	0
Other	0.02	−0.03	−0.01	0	0.02	−0.03	−0.02	0
Diurnal								
O1	−3.11	4.58	−0.16	−0.1	−3.18	4.69	−0.17	−0.1
Q1	−0.20	0.29	2.26	0	−0.18	0.26	2.06	0
θ-L-F	−0.11	0.16	−0.01	0.2	−0.11	0.17	−0.01	0.2
M1	−0.01	0.01	0.28	0	−0.01	0.01	0.33	0
J1	+0.01	−0.01	−0.18	0	0.01	−0.01	−0.31	0
$\theta - \Omega$	0	0	0	−0.2	0	0	0	−0.2
Other	−0.02	0.03	0.05	0	−0.02	0.02	0.03	0
Semidiurnal								
M2	−21.11	31.14	−1.10	−0.4	−20.92	30.86	−1.09	−0.4
N2	−1.50	2.21	17.22	0	−1.75	2.58	20.07	0
2N2	−0.04	0.06	0.74	0	−0.06	0.08	0.94	0
$2\theta - L - F$	−0.03	0.04	0	0.1	−0.03	0.04	0	0.1
$2\theta - 2L - 2D + l$	−0.05	0.08	−0.61	0.2	−0.06	0.09	−0.70	0.2
$2\theta - 2L - 2D$	−0.06	0.09	0	0.1	−0.08	0.11	0	0.2
L2	−0.01	0.01	−0.21	0	0	0.01	−0.14	0
Other	−0.01	0.01	0.08	0	−0.01	0.01	0.11	0

Table 10 continued

Tide	DE430 $dn/dt''/\text{cent}^2$	DE430 da/dt mm/year	DE430 de/dt 10^{-12}/year	DE430 di/dt μas/year	Soln D $dn/dt''/\text{cent}^2$	Soln D da/dt mm/year	Soln D de/dt 10^{-12}/year	Soln D di/dt μas/year
Moon								
Tide	0.21	−0.31	−4.55	−0.3	0.26	−0.39	−5.72	-0.4
Core	0.02	−0.03	0	−0.1	0.02	−0.02	0	-0.1
Total	−25.90	38.20	13.50	−0.5	−25.97	38.30	15.02	-0.5
	±0.03	±0.04		±0.1	±0.04	±0.05	±0.85	±0.1
	±0.05	±0.07		±0.1	±0.05	±0.08	±1.0	±0.1

The first set of uncertainties are internal uncertainties of the LLR fits; the second set includes conversion errors

Table 11 Summary of secular rates for a geophysical model, ephemeris DE430, and two recent LLR solutions

Source	dn/dt $''$/cent^2	da/dt mm/year	de/dt 10^{-12}/year	di/dt μas/year
Geophys. model				
Zonal	0.15	−0.22	−0.49	−0.03
Diurnal	−3.74	5.52	2.10	0.08
Semidiurnal	−22.83	33.68	15.92	−0.10
Earth total	−26.42	38.98	17.53	−0.05
DE430				
Zonal	0.12	−0.18	−0.32	−0.04
Diurnal	−3.44	5.08	2.24	0.06
Semidiurnal	−22.81	33.64	16.12	−0.06
Earth total	−26.13	38.54	18.04	−0.04
Moon tide	0.21	−0.31	−4.55	−0.33
Moon CMB	0.02	−0.03	0	−0.08
Total	−25.90	38.20	13.50	−0.45
Solution B				
Zonal	0.15	−0.22	−0.38	−0.05
Diurnal	−3.48	5.14	1.93	−0.01
Semidiurnal	−22.84	33.69	16.13	−0.06
Earth total	−26.17	38.60	17.68	−0.12
Moon tide	0.25	−0.37	−5.44	−0.40
Moon CMB	0.02	−0.03	0	−0.08
Extra de/dt			3.43	
Total	−25.90	38.21	15.67	−0.59
Solution D				
Zonal	0.15	−0.22	−0.38	−0.05
Diurnal	−3.49	5.15	1.94	−0.01
Semidiurnal	−22.91	33.78	19.19	0.03
Earth total	−26.25	38.71	20.74	−0.02
Moon tide	0.26	−0.39	−5.72	−0.42
Moon CMB	0.02	−0.02	0	−0.07
Total	−25.97	38.30	15.02	−0.51

For ±10 year from a reference time, the tidal perturbation in longitude is $-0.13''$ or −0.24 km. The monthly effect in radius is a factor of e smaller giving ±13 m, or somewhat more with solar perturbations. Since the LLR data for the last 20 year are fit with 1–2 cm scatter, the Eq. (10) tide model in the numerically integrated ephemeris represents the perturbation to ≤0.15 %, which is compatible with the stated uncertainties. The two τ_R solution values are negatively correlated such that an increase in one tidal acceleration component tends to be compensated by a decrease in the other. Consequently, the total uncertainty can be less than the uncertainties of the individual components.

There is a comparison value of dn/dt from independent software based on series expansions: Chapront et al. (2002) found an acceleration of $-25.858''$/cent^2 using the tidal acceleration model of Williams et al. (1978). The difference of only 0.4 % is encourag-

ing. Their terrestrial eccentricity rate was 15×10^{-12}/year, 17 % less than the DE430 value and 28 % less than our solution D, but with only a single terrestrial tidal acceleration parameter in their solution, de/dt was not independent of dn/dt. Also, Chapront et al. did not include tides on the Moon, which omission coincidently results in the correct total de/dt value. An LLR tidal solution by Aleshkina (2002) with the 1978 model and the foregoing $-1957\, k_2\, \Delta\theta$ conversion would give $-25.6''/\text{cent}^2$ for the terrestrial contribution; the questionable lunar contribution is perhaps 0.1 % more. With modern terrestrial and lunar models for tides, a recent LLR solution gives $dn/dt = -25.90''/\text{cent}^2$ (Pavlov et al. 2016), close to the DE430 and solution B values.

We prefer solution D since it accounts for the eccentricity rate. Including conversion uncertainty, its secular rates are $dn/dt = -25.97 \pm 0.05''/\text{cent}^2$, $da/dt = 38.30 \pm 0.08$ mm/year, $de/dt = (15.0 \pm 1.0) \times 10^{-12}$/year, and $di/dt = -0.5 \pm 0.1\ \mu$as/year. The tidal accelerations of longitude of perigee ϖ and node Ω are $0.383''/\text{cent}^2$ and $-0.101''/\text{cent}^2$, respectively.

Adjusting the Table 8 results to match the LLR diurnal and semidiurnal dn/dt, tidal deceleration of Earth rotation is $d\omega_E/dt = -1316''/\text{cent}^2$, or 87.5 s/cent^2 for angle-like UT1-AT, so that the length of day increases by 2.395 ms each century. Although LLR is not sensitive to the S2 contribution, which is ∼11 % of the total, we include that contribution. Krasinsky (1999) calculated a $d\omega_E/dt$ value that is 11 % less than our estimate due to use of an earlier smaller dn/dt. We note that there are historical nontidal changes in Earth rotation (Yoder et al. 1983; Stephenson and Morrison 1995; Cheng et al. 2013) due to a slowly decreasing moment of inertia. The tide-caused obliquity rate is predicted to be very small; it is much less than nontidal contributions.

8 Avoiding inadvertent accelerations

This section cautions that it is possible to get an erroneous acceleration of the Moon, or another synchronous body, by modeling approximations that involve the literal angles for L, l, or F. It is also possible for a small lunar orientation error to grow when integrating backward with CMB dissipation.

Newhall et al. (1983) described an erroneous acceleration in orbital longitude that became apparent during a long integration when the force model included a lunar gravity field that was oriented by a trigonometric series for physical librations. The lunar C_{22} gravity coefficient caused an acceleration of the form

$$\frac{d^2 \Delta L}{dt^2} \approx K^2 \Delta L, \tag{39}$$

where $\theta_M = L_S - \pi$ is the model orientation of the longitude of C_{22} by a series for mean longitude L_S, which includes polynomial and periodic terms. The difference between the real mean longitude and the series representation is $\Delta L = L - L_S$. An initial error in the constant term in the L_S polynomial will grow exponentially with an e-folding time of $1/K$ when integrated forward or backward. The expression for K is

$$K = 2n \frac{R}{a} \sqrt{3 C_{22} F_{220} G_{200}}, \tag{40}$$

where $G_{200} = 1 - 5e^2/2 + \cdots$ and $F_{220} = 3[1+\cos(i + I)]^2/4$ (Kaula 1966) and the tilt of the lunar equator plane to the ecliptic plane is $i + I = 6.7°$. For the Moon, $1/K = 93$ year. Linear and quadratic errors in the L_S polynomial would also grow exponentially.

The forgoing problem motivated us to integrate the physical librations along with the orbit (Newhall et al. 1983). The free mode for longitude libration about synchronous rotation is oscillatory with a 2.9 year period (Rambaux and Williams 2011). Since 2.9 year <<93 year, the equations of motion do not have an instability when orbit and orientation are integrated together. The Moon's synchronous rotation follows slow variations (periods >>2.9 year) of orbit longitude including the tidal acceleration. See Newhall et al. for further details.

Can a similar problem arise if the terrestrial tides are represented with an analytical series in the integration model? As a rough approximation we write

$$\frac{\mathrm{d}^2 L}{\mathrm{d}t^2} \propto \sin\left(2L - 2L_S - \chi\right) \tag{41}$$

where L_S is the angle L approximated by a polynomial and χ is a phase shift. Then with $\Delta L = L - L_S$

$$\frac{\mathrm{d}^2 \Delta L}{\mathrm{d}t^2} \approx -\sin\left(2\Delta L\right) \cot \chi \frac{\mathrm{d}n}{\mathrm{d}t} \tag{42}$$

With tidal $\mathrm{d}n/\mathrm{d}t = -26''/\mathrm{cent}^2$ and a phase shift of 0.077 radians, the error ΔL has an exponential growth forward or backward with an e-folding time of 1750 year. Long integrations would have an instability in the equations of motion. Although the e-folding time will depend on the nature of the analytical model, such an instability would affect integrations longer than about one millennium. Integrations with tides represented by series should be accurate for the length of the LLR data span, e.g., the IERS case in Pavlov et al. (2016).

In addition to tidal dissipation, the model of the JPL integrator includes energy dissipation between the moving fluid and the solid mantle at the lunar core-mantle boundary (CMB) (Williams et al. 2001; Standish and Williams 2013; Folkner et al. 2014). Dissipation causes damping of the free libration modes when integrating forward (Williams et al. 2001), but exponential growth when integrating backward. Also, dissipation causes most free libration amplitudes to damp with 10^4 to 10^6 year times scales. These modes are periodic. One rotation mode connected to CMB dissipation damps with a century time scale. It acts in a secular manner. Owing to coupling through the lunar C_{22}, the orbit is also corrupted for times exceeding a century. To avoid problems with the backward integration, a long forward and backward integration DE431 excluded CMB damping in the LLR solution and integration (Folkner et al. 2014) despite degradation of the rms residual during the LLR fit. For modern lunar data analysis, ephemeris DE430 with CMB damping has been our lunar standard since 2013 (Williams et al. 2013; Folkner et al. 2014). The integration starts in 1969. From a comparison between DE430 and DE431, the longitude difference is $<0.1''$ at 1800, $<0.2''$ at 1600, and $\sim 0.3''$ at 1550. Unlike the forgoing differences that have both signs, the differences going forward appear to be quadratic with time growing by $<0.02''/\mathrm{cent}^2$. These errors in the lunar orbit should be considered when analyzing older accurate data with DE431.

9 Comments

In the absence of dissipation, there is little to cause secular changes the lunar semimajor axis (Poisson's theorem). Nevertheless, there is a classical acceleration in lunar mean longitude and rate of change of mean motion due mainly to the secular change in the eccentricity of the solar orbit; Chapront-Touzé and Chapront (1983, 1988) give $12.1''/\mathrm{cent}^2$ with respect to the J2000 equinox. There are also classical accelerations of longitude of perigee and node: $-76.9''/\mathrm{cent}^2$ and $12.8''/\mathrm{cent}^2$, respectively. The tidal accelerations of the three angles add

on to the classical accelerations. For motions with respect to the precessing equinox, an acceleration of $-2.2''/\text{cent}^2$ should be subtracted.

Dissipation laws for tides in the Moon have been discussed by Williams and Boggs (2015). The time delay and Maxwell viscosity laws were poor matches to dissipation over a spread of lunar tidal periods. The best performing laws had a peak at a few months. The use of a time delay model in the integrator is only justified by convenience of implementation. By dividing the terrestrial dissipation into three frequency bands and using a variable delay for two of them, our tidal acceleration model in the integrator minimizes many problems with the time delay approach. Tides in the Moon are more of a problem since the three degree-2 and order-m components do not give separate frequency bands and the frequency spread is similar to zonal tides on the Earth. The amount of lunar energy dissipation is strongest for monthly periods so the time delay approach should be adequate for the orbit, but the effect of dissipation on the physical librations with their wide spread of periods presents a problem. See Williams and Boggs for the affected libration expressions that require special treatment. There may be a wide variety of dissipation behavior in various exoplanets; see the discussion in Henning et al. (2009) and references therein.

An unmodeled extra or anomalous eccentricity rate of 3×10^{-12} /year has been a puzzle. It is reduced from earlier larger values (Williams and Boggs 2009; Williams et al. 2014a) to its present size from improved tidal modeling and correction of a missing factor of 2 in its partial derivative. The extra rate would be removed if the phase of the N2 tide were increased. A study of the influence of two tidal acceleration models on de/dt is given by Pavlov et al. (2016). Although it is possible to construct a hypothetical radial acceleration that causes a secular eccentricity rate (Iorio 2011), searches for gravitational physics or cosmological causes of eccentricity rate have not been fruitful (Iorio 2011, 2014). A geophysical cause is a welcome explanation.

A rapidly spinning solid planet with a fluid core has a resonance in its tidal distortion due to the oblate CMB. A tidal resonance will exist in the diurnal band. For the Earth, the resonance is offset from 1 cycle per sidereal day by 1/(14 months). This puts it near the K1 tide at the sidereal day period; Table 6 and Fig. 1 shows the effect on the Love number. There are weaker tides, e.g., ψ 1 with argument $\theta + l'$, closer to the resonance.

The evolving Earth–Moon system provides an example of tidal evolution that is relevant to other solar system bodies and exoplanets beyond. The Earth with its oceans is a slowly varying source of tidal dissipation. The continents move at a few cm/year, comparable to lunar tidal recession. Consequently, the ocean basins change shape and the strengths of the zonal, diurnal, and semidiurnal tides change. The present widely separated Pacific and Atlantic oceans couple to the 2,2 tides more strongly than a hemispheric (degree 1) ocean shape would. Poliakow (2005) calculates that the M2 tidal dissipation has varied by a factor of eight during the past 570 million years with the present lunar tidal evolution faster than the past interval. With the adjusted N2 phase, the present negative de/dt from the Moon is $\sim$1/4 of the positive terrestrial rate. Therefore, we infer that the total eccentricity rate can be negative when terrestrial dissipation is very low and positive when it is high. Because of the changing oceans, the rate of evolution of all orbit elements and Earth orientation parameters will vary by large amounts.

For times that are long compared to the separation of the continents, evolution slows down as the semimajor axis increases. The ocean response has a complicated set of resonances. Dissipation in the oceans depends on the placement of the resonant frequencies with respect to the rotation rate; a past faster spinning Earth was less effective with a larger Q (Webb 1982; Hansen 1982; Bills and Ray 1999). Finally, we note that tidal dissipation in the body

of the Earth and Moon will depend on their thermal evolution, which is fastest during their early history (Meyer et al. 2010).

What can be improved? The internal accuracy of dn/dt, da/dt, and de/dt will improve as the LLR data span gets longer. The computations for the conversion of tidal parameters into de/dt can be improved. The S_W correction in Eq. (26) could be improved with a better value for the long time (zero shear strength) spherical component. This paper has restricted itself to secular changes. There are long period terms that we have not explored. We no longer recommend the idealized model of Williams et al. (1978), but that paper indicates that there are 18.6 year terms in longitude of a few milliarcsecond size that are big enough to be useful. These long period terms should be present in our integrations; presumably they allow the separation of the diurnal and semidiurnal tides during fits of LLR data.

10 Summary

The degree-2 tidal potential at the Earth that arises from the gravitational attraction of the Moon and Sun is discussed in Sect. 2. Expressed as a tide raising potential, the tidal forces cause a deformation of the Earth that induces an additional tidal potential. At its simplest, this responding potential is equal to the tide raising potential multiplied by Love number k_2. To approximate a complicated Earth, the potential is expressed with spherical harmonic functions and the k_2 factor is split up into k_{2m}, where m is the spherical harmonic order 0, 1, or 2. To allow for dissipation, time delays τ_m can be introduced.

The numerical integration of the lunar orbit requires tide caused accelerations. The gradient of the responding potential with three Love numbers and three time delays has been used in the past (Standish and Williams 2013), but we introduce more flexibility by setting up three separate time delays for orbit and two for Earth rotation. The terrestrial phase shifts depend on tidal period and the two extra delays allow the diurnal and semidiurnal tidal phase lags to vary linearly with frequency. The resulting tidal acceleration that is presented by Eq. (10) is used in the JPL programs that integrate the orbits of the Moon and planets (Folkner et al. 2014).

The accuracy and time span of the lunar laser ranging (LLR) data have improved over the past 46 year. Consequently, the tidal acceleration model for our numerical integration of the lunar orbit (Folkner et al. 2014) has become more sophisticated. Our tidal acceleration model combines the effect of ocean tides with Earth tides. Although much less sophisticated than the tidal model needed for lower Earth satellites (Petit and Luzum 2010), integrations with Eq. (10) are able to fit the last 20 year of LLR data at the 1–2 cm accuracy level.

Separate from a practical tidal model for the numerical integration program, a more analytical approach is given in Sect. 3. Fourier series for the tidal potential are developed. Series for a set of related matrix functions $U_{ij}(t)$ are given in Table 1. The series for the tidal potential expressed as terrestrial gravitational $\Delta C_{2m}(t)$ and $\Delta S_{2m}(t)$ are computed from the U_{ij} in Eqs. (21–25) and given in Tables 3, 4 and 5. The ΔC_{2m} and ΔS_{2m} in the Earth's rotating frame are useful because the distortions of the Earth and oceans respond to the frequencies in the rotating frame. The Love numbers and time delays can be represented as functions of tidal period P with a complex $k_{2m}{}^*(P)$.

There are measurements of the larger Earth and ocean tidal components and geophysical models for the smaller ones. Model values of $k_{2m}{}^*(P)$ are presented in Table 6 of Sect. 4 for a selection of major components. For numerical integrations, the choice of three Love numbers and three time delays are partly based on the table.

Converting the Love number and time delay parameters to the familiar secular dn/dt, da/dt, and de/dt is separate from both the numerical integration and data fitting. Section 5 presents the conversion equations and Table 7 gives their numerical evaluations. Apart from the internal error for secular tidal rates, the equations for conversion of rates come with their own uncertainties. For dn/dt and da/dt that uncertainty is estimated to be ∼0.15 %, but for de/dt it is likely several percent.

The geophysical parameters in Table 6 are combined with conversion Table 7 to derive model values of dn/dt, da/dt, and de/dt for each terrestrial component. These secular tidal rates are tabulated in Table 8 of Sect. 5.3 along with model rates for rotation $d\omega_E/dt = -1325''/\text{cent}^2$ and obliquity $d\epsilon/dt = 9$ μas/year.

The DE430 solution (43 year span) and two new (45 year) LLR solutions are presented in Table 9 and discussed in Sect. 6. As a result of the geophysical model in Table 6, one Love number and several delays have changed since the earlier work. One new solution adds an extra $de/dt \approx 3 \times 10^{-12}$/year of unspecified origin and another adjusts an additional time delay; both improve the fits. The extra de/dt is absorbed by increasing the phase of the N2 tide in the last solution.

The LLR Love numbers and time delays are converted into secular rates in Sect. 7 and the contributions of components are presented in Table 10. A summary is given in Table 11 for the geophysical model, DE430, and two new solutions. Including both LLR fit and conversion uncertainties, the preferred new solution gives secular rates $dn/dt = -25.97 \pm 0.05''/\text{cent}^2$, $da/dt = 38.30 \pm 0.08$ mm/year, $de/dt = (15.0 \pm 1.0) \times 10^{-12}$/year, and $di/dt = -0.5 \pm 0.1$ μas/year. Decreasing the Table 8 result to better match the LLR solution for dn/dt, the computed tidal deceleration of Earth rotation is $d\omega_E/dt = -1316''/\text{cent}^2$ or 87.5 s/cent^2 for UT1-AT so that the length of day increases 2.395 ms each century. Note that there is also a sizable non-tidal acceleration of Earth rotation (Stephenson and Morrison 1995).

In Sect. 8 we describe how to avoid several possible sources of false acceleration from the model in the integrator. Generally, for long time fidelity the acceleration model should not include an analytical expression for the lunar longitude when orienting the Moon or computing tides. Also, dissipation at the lunar core mantle boundary causes a growing error when integrating backward.

The LLR tidal dissipation results provide a test of the geophysical information on dissipation. Compared to the information in Sect. 4 and Tables 6 and 11, the LLR and geophysical results for tidal energy dissipation disagree by ≤1 %, but most of that difference is in the diurnal dissipation, which is 7–9 % smaller for the LLR results. The detected eccentricity rate can be accommodated by increasing the phase of the N2 tide. During the past evolution of the orbit, the eccentricity rate may have been negative during times of low terrestrial dissipation (Sect. 9).

Acknowledgments We thank the lunar laser ranging stations at McDonald Observatory, Texas, Observatoire de la Côte d'Azur, France, Haleakala Observatory, Hawaii, Apache Point Observatory, New Mexico, and Matera, Italy that provided the data sets that make LLR analyses possible. LLR data are available from the International Laser Ranging Service archive at http://ilrs.gsfc.nasa.gov/. We acknowledge extensive conversations with D. Pavlov about tidal modeling that benefited this paper. C. F. Yoder contributed to the early development of the solar perturbation scaling factors for LLR results. M. Efroimsky provided a valuable review. The research described in this paper was carried out at the Jet Propulsion Laboratory of the California Institute of Technology, under a contract with the National Aeronautics and Space Administration. Government sponsorship acknowledged.

Appendix

List of symbols

a	Semimajor axis of lunar orbit
a'	Semimajor axis of solar orbit
C	Moment of inertia
C_{2m}	Gravity field coefficients
D	Mean elongation of Moon from Sun
e	Eccentricity of lunar orbit
F	Lunar mean argument of latitude
G	Gravitational constant
h_2	Vertical Love number
i	Lunar inclination to ecliptic plane
k_2	Potential Love number
K_V	Parameter for dissipation at lunar CMB
l	Lunar mean anomaly
l'	Solar mean anomaly
L	Lunar mean longitude
L'	Solar mean longitude
m	Order
M_E	Mass of Earth
M_M	Mass of Moon
M_S	Mass of Sun
M'	Mass of external body
n	Sidereal mean motion of Moon
n'	Sidereal mean motion of Sun
P	Period
P_{2m}	Associated Legendre polynomial
q	Index for different periods in Fourier series
r	Distance from center of Earth to body
R	Radius of Earth
S	Scaling parameters near unity
S_{2m}	Gravity field coefficient
t	Time
u_i	Unit vector from Earth to external body
U_{ij}	Functions $(a/r)^3 u_i u_j$
U_{ijq}	Periodic term of U_{ij}
V_2	Potential from tidal distortion
W_2	Tide raising potential
α	Right ascension
ε	Obliquity
Δ	Small difference
ΔC_{2m}	Degree-2 tidal gravity field coefficients
ΔS_{2m}	Degree-2 tidal gravity field coefficients
Θ	Earth-centered angle between an external body and a selected point
ϑ	Rotation angle between precessing equinox and zero longitude
λ	Terrestrial longitude
τ_0	Zonal time delay

τ_1	Diurnal time delay for orbit
τ_2	Semidiurnal time delay for orbit
τ_{R1}	Diurnal time delay for rotation
τ_{R2}	Semidiurnal time delay for rotation
τ_M	Time delay for tides on Moon
χ	Phase lag
ω	Lunar mean argument of perigee
ω_E	Spin rate of Earth
Ω	Lunar mean node
ϖ	Lunar longitude of perigee $\Omega+\omega$
ζ	Angular argument

References

Aleshkina, E.Y.: Lunar numerical theory and determination of parameters k_2, δ_M from analysis of LLR data. Astron. Astrophys. **394**, 717–721 (2002). doi:10.1051/0004-6361:20021149

Bills, B.G., Ray, R.D.: Lunar orbital evolution: a synthesis of recent results. Geophys. Res. Lett. **26**, 3045–3048 (1999). doi:10.1029/1999GL008348

Brown, E.W.: An introductory treatise on the lunar theory. Cambridge University Press, Cambridge (1896)

Brown, E.W.: Tables of the motion of the Moon. Yale University Press, New Haven (1919)

Capitaine, N., Wallace, P.T., Chapront, J.: Expressions for IAU 2000 precession quantities. Astron. Astrohys. **412**, 567–586 (2003). doi:10.1051/0004-6361:20031539

Chapront, J., Chapront-Touzé, M.: Lunar motion: theory, and observations. Celesti. Mech. Dyn. Astron. **66**, 31–38 (1996). doi:10.1007/BF00048821

Chapront-Touzé, M.: Perturbations due to the shape of the Moon in the lunar theory ELP 2000. Astron. Astrophys. **119**, 256–260 (1983)

Chapront-Touzé, M., Chapront, J.: The lunar ephemeris ELP 2000. Astron. Astrophys. **124**, 50–62 (1983)

Chapront-Touzé, M., Chapront, J.: ELP 2000–85: a semi-analytical lunar ephemeris adequate for historical times. Astron. Astrophys. **190**, 342–352 (1988)

Chapront-Touzé, M., Chapront, J.: Lunar Tables and Programs from 4000 B. C. to A. D. 8000. Willmann-Bell, Richmond (1991)

Chapront, J., Chapront-Touzé, M., Francou, G.: A new determination of lunar orbital parameters, precession constant and tidal acceleration from LLR measurements. Astron. Astrophys. **387**, 700–709 (2002)

Cheng, M., Tapley, B.D., Ries, J.C.: Deceleration in the Earth's oblateness. J. Geophys. Res. **118**, 740–747 (2013). doi:10.1002/jgrb.50058

Christodoulidis, D.C., Smith, D.E., Williamson, R.G., Klosko, S.M.: Observed tidal breaking in the Earth/Moon/Sun system. J. Geophys. Res. **93**, 6216–6236 (1988). doi:10.1029/JB093iB06p06216

Deprit, A., Henrard, J., Rom, A.: Analytical lunar ephemeris: Delaunay's theory. Astron. J. **76**, 269–272 (1971)

Dickey, J.O., Bender, P.L., Faller, J.E., Newhall, X.X., Ricklefs, R.L., Ries, J.G., et al.: Lunar laser ranging: a continuing legacy of the Apollo program. Science **265**, 482–490 (1994). doi:10.1126/science.265.5171.482

Eckert, W.J., Jones, R., Clark, H.K.: Construction of the lunar ephemeris, in Improved Lunar Ephemeris 1952–1959. A Joint Supplement to the American Ephemeris and the (British) Nautical Almanac. U. S. Naval Observatory, U. S. Government Printing Office, pp. 283–363 (1954)

Folkner, W.M., Williams, J.G., Boggs, D.H., Park, R.S., Kuchynka, P.: The planetary and lunar ephemerides DE 430 and DE431. The Interplanetary Network (IPN) Progress Report 42-196, Feb 15, 2014, Jet Propul. Lab., Pasadena, Calif. (2014). http://ipnpr.jpl.nasa.gov/progress_report/42-196/196C.pdf

Hansen, K.S.: Secular effects of oceanic tidal dissipation on the Moon's orbit and the Earth's rotation. Rev. Geophys. Space Phys. **20**, 457–480 (1982). doi:10.1029/RG020i003p00457

Hartmann, T., Wenzel, H.-G.: The HW95 tidal potential catalogue. Geophys. Res. Lett. **22**, 3553–3556 (1995). doi:10.1029/95GL03324

Henning, W.G., O'Connell, R.J., Sasselov, D.D.: Tidally heated terrestrial exoplanets: viscoelastic response models. Astrophys. J. **707**, 1000–1015 (2009). doi:10.1088/0004-637X/707/2/1000

Henrard, J.: Analytic lunar ephemeris: a report. Publication of the department of mathematics. University of Namur, Belgium (1972)

Hilton, J.L., Capitaine, N., Chapront, J., Ferrandiz, J.M., Fienga, A., Fukushima, T., et al.: Report of the international astronomical union division I working group on precession and the ecliptic. Celesti. Mech. Dyn. Astron. **94**(3), 351–367 (2006). doi:10.1007/s10569-006-0001-2

Iorio, L.: On the anomalous secular increase in the eccentricity of the orbit of the Moon. Mon. Not. R. Astron. Soc. **415**, 1266–1275 (2011). doi:10.1111/j.1365-2966.2011.18777.x

Iorio, L.: An empirical explanation of the anomalous increases in the astronomical unit and the lunar eccentricity. Astron. J. **142**(68), 1–3 (2011b). doi:10.1088/0004-6256/142/3/68

Iorio, L.: The lingering anomalous secular increase in the eccentricity of the orbit of the Moon: further attempts of explanation of cosmological origin. Galaxies **2**(2), 259–262 (2014). doi:10.3390/galaxies2020259

Kaula, W.M.: Tidal dissipation by solid friction and the resulting orbital evolution. Rev. Geophys. **2**, 661–685 (1964). doi:10.1029/RG002i004p00661

Kaula, W.M.: Theory of Satellite Geodesy. Dover Publications Inc, Mineola, New York, p. 124. (1966)

Konopliv, A.S., Park, R.S., Yuan, D.-N., Asmar, S.W., Watkins, M.M., Williams, F.G., et al.: The JPL lunar gravity field to spherical harmonic degree 660 from the GRAIL primary mission. J. Geophys. Res. **118**, 1415–1434 (2013). doi:10.1002/jgre.20097

Krasinsky, G.A.: Tidal effects in the Earth–Moon system and the Earth's rotation. Celesti. Mech. Dyn. Astron. **75**, 39–66 (1999). doi:10.1023/A:1008381000993

Lemoine, F.G., Goossens, S., Sabaka, T.J., Nicholas, J.B., Mazarico, E., Rowlands, D.D., et al.: High-degree gravity models from GRAIL primary mission data. J. Geophys. Res. Planets **118**, 1676–1698 (2013). doi:10.1002/jgre.20118

Lyard, F., Lefevre, F., Letellier, T., Francis, O.: Modeling the global ocean tides: modern insights from FES2004. Ocean Dyn. **56**, 394–415 (2006). doi:10.1007/s10236-006-0086-x

Mathews, P.M., Herring, T.A., Buffet, B.A.: Modeling of nutation and precession: New nutation series for non-rigid Earth and insights into the Earth's interior. J. Geophys. Res. **107** (B4), ETG 3-1–ETG 3-26 (2002). doi:10.1029/2001JB000390

Meyer, J., Elkins-Tanton, L., Wisdom, J.: Coupled thermal-orbital evolution of the early Moon. Icarus **208**, 1–10 (2010). doi:10.1016/j.icarus.2010.01.029 Corrigendum to Coupledthermal-orbital evolution of the early Moon. doi:10.1016/j.icarus.2010.12.008

Mignard, F.: The lunar orbit revisited, III. Moon Pl. **24**, 189–207 (1981). doi:10.1007//BF00910608

Murphy Jr., T.W., Adelberger, E.G., Battat, J.B.R., Carey, L.N., Hoyle, C.D., LeBlanc, P., et al.: APOLLO: The Apache point observatory lunar laser-ranging operation: instrument description and first detections. Publ. Astron. Soc. Pacific **120**, 20–37 (2008). doi:10.1086/526428, arXiv:0710.0890 [astro-ph]

Murphy Jr., T.W., Adelberger, E.G., Battat, J.B.R., Hoyle, C.D., Johnson, N.H., McMillan, R.J., et al.: APOLLO: millimeter lunar laser ranging. Class. Quantum Grav. **29**, 184005 (2012). doi:10.1088/0264-9381/29/18/184005

Murphy, T.W.: Lunar laser ranging: the millimeter challenge. Rep. Prog. Phys. **76**, 076901 (2013). doi:10.1088/0034-4885/76/7/076901

Newhall, X.X., Standish, E.M., Williams, J.G.: DE 102, a numerically integrated ephemeris of the Moon and planets spanning forty-four centuries. Astron. Astrophys. **125**, 150–167 (1983)

Pavlov, D.A., Williams, J.G., Suvorkin, V.V.: Determining parameters of Moon's orbital and rotational motion from LLR observations using GRAIL and IERS-recommended models. Submitted to Celest. Mech. Dyn. Astron. (2016) (in press)

Petit, G., Luzum, B.: IERS Conventions (2010). IERS Tech. Note 36, pp. 179, Verlag des Bundesamts für Kartographie und Geodäsie, Frankfurt am Main (2010). http://www.iers.org/TN36/

Poliakow, E.: Numerical modeling of the paleotidal evolution of the Earth-Moon system. In: Proceedings of International Astronomical Union Colloquium 197. Dynamics of Populations of Planetary Systems. August–September 2004, Belgrade. Edited by Knezevic, Z., Milani, A., Cambridge Univ. Press, pp. 445–452 (2005). doi:10.1017/S174392130400897X

Rambaux, N., Williams, J.G.: The Moon's physical librations and determination of their free modes. Celesti. Mech. Dyn. Astron. **109**, 85–100 (2011). doi:10.1007/s10569-010-9314-2

Ray, R.D., Eanes, R.J., Lemoine, F.G.: Constraints on energy dissipation in the Earth's body tide from satellite tracking and altimetry. Geophys. J. Int. **144**, 471–480 (2001). doi:10.1046/j.1365-246x.2001.00356.x

Ray, R.D., Erofeeva, S.Y.: Long-period tidal variations in the length of day. J. Geophys. Res. Solid Earth **119**, 1498–1509 (2014). doi:10.1002/2013JB010830

Rubincam, D.P.: Tidal friction in the Earth–Moon system and Laplace planes: Darwin redux. Icarus **266**, 24–43 (2016). doi:10.1016/j.icarus.2015.10.024

Samain, E., Mangin, J.F., Veillet, C., Torre, J.-M., Fridelance, P., Chabaudie, J.E., et al.: Millimetric lunar laser ranging at OCA (Observatoire de la Côte d'Azur). Astron. Astrophys. Suppl. Ser. **130**, 235–244 (1998). doi:10.1051/aas:1998227

Simon, J.L., Bretagnon, P., Chapront, J., Chapront-Touzé, M., Francou, G., Laskar, J.: Numerical expressions for precession formulae and mean elements for the Moon and planets. Astron. Astrophys. **282**, 663–683 (1994)

Standish, E.M., Williams, J.G.: Orbital ephemerides of the Sun, Moon, and planets. Chapter 8. In: Urban, S., Seidelmann, P.K. (eds.) Explanatory Supplement to the Astronomical Almanac, 3rd edition, pp. 305–345. University Science Books, Mill Valley, CA (2013). http://iau-comm4.jpl.nasa.gov/XSChap8.pdf

Stephenson, F.R., Morrison, L.V.: Long-term fluctuations in the Earth's rotation: 700 BC to AD 1990. Philos. Trans. R. Soc. **351**, 165–202 (1995). doi:10.1098/rsta.1995.0028

Webb, D.J.: Tides and the evolution of the Earth–Moon system. Geophys. J. R. Astron. Soc. **70**, 261–271 (1982). doi:10.1111/j1365-246X.1982tb06404.x

Williams, J.G., Sinclair, W.S., Yoder, C.F.: Tidal acceleration of the Moon. Geophys. Res. Lett. **5**, 943–946 (1978). doi:10.1029/GL005i011p00943

Williams, J.G.: Contributions to the Earth's obliquity rate, precession, and nutation. Astron. J. **108**, 711–724 (1994). doi:10.1086/117108

Williams, J.G., Boggs, D.H., Yoder, C.F., Ratcliff, J.T., Dickey, J.O.: Lunar rotational dissipation in solid body and molten core. J. Geophys. Res. **106**, 27933–27968 (2001). doi:10.1029/2000JE001396

Williams, J.G., Boggs, D.H.: Lunar core and mantle. What does LLR see? In: Proceedings of 16th International Workshop on Laser Ranging, SLR—the Next Generation, October 2008, Poznan, Poland, ed. Stanislaw Schillak, pp. 101–120 (2009). http://www.astro.amu.edu.pl/ILRS_Workshop_2008/index.php

Williams, J.G, Boggs, D.H., Folkner, W.M.: DE430 Lunar Orbit, Physical Librations, and Surface Coordinates. IOM 335-JW,DB,WF-20130722-016, July 22, 2013, Jet Propul. Lab., Pasadena, Calif. (2013). http://naif.jpl.nasa.gov/pub/naif/generic_kernels/spk/planets/de430_moon_coord.pdf

Williams, J.G., Turyshev, S.G., Boggs, D.H.: The past and present Earth-Moon system: the speed of light stays steady as tides evolve. Planet. Sci. **3**, 2 (2014a). doi:10.1186/s13535-014-0002-5. http://www.planetary-science.com/content/3/1/2

Williams, J.G., Konopliv, A.S., Boggs, D.H., Park, R.S., Yuan, D.-N., Lemoine, F.G., et al.: Lunar interior properties from the GRAIL mission. J. Geophys. Res. Planets **119**, 1546–1578 (2014b). doi:10.1002/2013JE004559

Williams, J.G., Boggs, D.H.: Tides on the Moon: theory and determination of dissipation. J. Geophys. Res. Planets **120**(4), 689–724 (2015). doi:10.1002/2014JE004755

Yoder, C.F., Williams, J.G., Sinclair, W.S., Parke, M.E.: Tidal variations of Earth rotation. J. Geophys. Res. **86**, 881–891 (1981). doi:10.1029/JB086iB02p00881

Yoder, C.F., Williams, J.G., Dickey, J.O., Schutz, B.E., Eanes, R.J., Tapley, B.D.: Secular variation of Earth's gravitational harmonic J2 coefficient from Lageos and the nontidal acceleration of Earth rotation. Nature **303**, 757–762 (1983). doi:10.1038/303757a0